Structure and dynamics of modulated colloids: Theoretical studies

Thesis submitted for the degree of

Doctor of Philosophy (Science)

in

Physics (Theoretical)

by

Suravi Pal

Department of Physics

University of Calcutta

2024

Acknowledgments

I would like to express my immense gratitude towards my supervisors, Professor Professor Jaydeb Chakrabarti and Professor Srabani Chakrabarty nee Sarkar. I hold myself extremely fortunate to have been obtaining the opportunity to work under the supervision of such brilliant minds. Their dedication, immense knowledge, and patience have been the key factors for producing a successful thesis out of me. I am highlly indebted to Professor Jaydeb Chakrabarti for accepting my PhD application and offerring me this unique opportunity to carry out my work at the S. N. Bose National Centre for Basic Sciences. Both my supervisors have enriched me in valuable scientific and life lessons. I also thank the members of my PhD research committee, Professor Shakuntala Chatterjee and Professor Gautam Gangopadhyay, for their very insightful comments throughout my evaluations in due course of PhD work. I also express my gratitude towards the reviewers who have taken precious time out to review this thesis. I shall be highly benefitted from their valuable comments.

I acknowledge financial support from S. N. Bose National Centre for Basic Sciences, through DST PhD fellowship. My humble gratitude towards all the academic and non-academic staffs of S.N. Bose National Center for Basic Sciences, for their timely and efficient issuance of all official papers that I needed from time to time.

Lastly, my immense thanks to my seniors, Dr Sashthi Charan Mondal, Dr Abhik Ghosh Moulick, Dr Rahul Karmakar, Dr Sutapa Dutta, Dr Edwine Tendong and my juniors Anirban Paul, Kanika Kole, Avik Sasmal, Sabuj and Anusree Sen for helping me in many stimulating discussions all throughout my PhD career.

Chapter 1: Introduction

Colloids are macro-molecular systems consisting of large ($1 \sim 1-10\mu m$) particles suspended typically in water. Due to large size and slow timescale they provide unique opportunity to explore condensed phase properties following the individual particle motions via laser light scattering and optical microscopy [1–5]. Colloids can be easily perturbed by external modulation which make them suitable for industrial application as well. We present this thesis primarily focusing on the structural and dynamic properties of modulated colloids. We probe the dynamical behaviour of a mono-disperse colloidal system in 2D modulated by an external potential in one direction. We look into its structural and dynamical properties.

We observe dynamic anisotropy caused by external modulation in the particle arrangement as they align themselves along the potential minima. This alignment results in arrested motion along the modulation direction. We observe both faster and slower particles along the potential minima as the confinement gets stronger with increasing external modulation. Thus, the dynamics become heterogeneous due to hinderence faced by the particles along the potential because of the arrested motion along the modulation direction.

We further consider a binary mixture of particles with size ratio 2:1 and interacting via repulsive interaction. We observe phase separation as a result of strong intra-species repulsion in absence of modulation. We apply a spatially periodic potential with wavelength matching with the diameter of the bigger particles and stronger for them. As a result, the bigger particles get aligned along the potential minima. While arranging themselves in this fashion, they break the big clusters of the smaller particles, mixing the components. The mixing tendency gets enhanced as we increase the strength of the external modulation. We observe that the mixing phenomena is accompanied by a first order phase transition reflected in jump in order parameter and peak in specific heat. The dynamics become slow due to arrested motion of the particles along the potential minima. We then start with the modulated mixed binary system and turn off the external modulation. We study the system evolving in time. We observe that big clusters of smaller particles appear in the system due to mutual intra-species repulsion. In the transient state, the big particles diffuse faster with time, while the smaller particles get slower.

We organise this chapter as follows: We present a brief review of works done in colloids in past decade in and out of equilibrium in section II. Section III highlights the main results from works done in modulated colloids. We then describe our work in nutshell on modulated binary colloids in section III and IV.

I. COLLOIDAL SUSPENSIONS

A colloidal solution is a homogeneous dispersion of particles having diameter within the range 1 to 10 μm. The particle motion is characterised by Brownian motion. Colloids are often found in nature in the form of aerosols, blood corpusles etc, whereas can be synthesized as polysterene beads artificially in laboratory. Colloids are synthesized in laboratory very easily and are realizable using video microscopy due to their large lengthscale and slow timescale. This enables scientists to model many fundamental problems in condensed matter and statistical physics, such as freezing and melting, crystal neucleation, glass transition and so on. Here we summarise some studies on colloidal dispersions.

Mono-disperse colloidal system with tunable parameter to distinguish between hard and soft sphere model has been studied experimentally[6]. The study demonstrates a 3D charged colloidal suspension of spheres in a mixture of cycloheptyl bromide and decalin. The colloids are taken such that the repulsion range and the anisotropy of the interparticle interaction potential can be controlled. Crystallisation is observed for higher volume fraction in case of hard spheres, it occurs at lower volume fraction for soft spheres. Expelimentalists explore this phase behaviour in real space by confocal microscopy. Colloids are very well known entities for self-organisation and self-assembly under various tunable parameters. One such experiment demonstrates structural motifs using bidisperse charged colloids[7]. Another work illustrates rich structure fabricated by depleting silica on liqiud crystals[8, 9]. They self-assemble to create intricate structures by deformation induced by osmotic stresses. Many experiments nowadays aim to achieve 3D colloidal structure with diamond symmetry[10]. Different type of colloidal packing has been of interest in recent years [11]. An experimental study attached small numbers of colloidal microspheres surfaces of liquid emulsion droplets. While removing fluid from the droplets, packings of spheres has been observed. The packings show a wide range of structures starting from sphere doublets, triangles, and tetrahedra to exotic polyhedra which are not found in infinite lattice packings. Experimental study with direct measurements on highly charged polystyrene spheres has been reported[12]. The polysterene spheres have been subjected to confinement, which leads to long-ranged attraction. The spheres sedimented into a monolayer above glass surface. This study also characterizes the equilibrium pair potential.

Experiments on colloids out of equilibrium have also been reported [13]. Optical traps have been used to held two colloidal probe particles. Bath particles are excluded from going to one probe from another at sufficiently close separations. This results in an asymmetric, non-equilibrium microstructure. Depletion like features of the region in between the probes are well explored in out of equilibrium. Time-resolved fluorescence confocal scanning microscopy

has enabled to directly study the dynamics of colloidal system modelled as hard spheres[14]. The study takes up a 2D dense liquid and vary the volume fraction to observe dynamical heterogeneity in the system.

Simulations by means of hard or soft sphere model of colloids have proved insights to many rich phase and dynamic behaviour of condensed matter systems. Techniques to simulate these models are well established in books by Allen & Tildesley[15] and by Frenkel & Smit[16]. The simulations over the years are carried out successfully by tracing out the huge number of degrees of freedom of atoms showed by the solvent molecules. In this way, one can model colloidal system taking into account their systematic interactions and other necessary parameters relevant to the system specific simulations. Colloids with high volume fraction under a magnetic field are simulated to form long chains[17]. The study also explore the interactions among those chains. Another study probe into phase diagram of ferrocoloid with permanant moments suspended in non-dissociated liquid[18]. The higher strength of an applied magnetic field favours phase separation. Charged colloids dominated by electrostatic interactions have been studied extensively. Recent advances characterising a system with primitive model of electrolytes has been reviewed explicitly[19]. The review focuses on four representative colloidal systems, namely spherical cell model, cylindrical cell model containing two colloids and structural and theromodynamic properties have been explored for a colloidal system in a cubic box with periodic boundary considtions. A wide review of such works in colloids has been presented earlierref.

II. MODULATED COLLOID

Colloidal macro-molecules are intriguing, for they are easily perturbed by external agents, like laser field[20], electric field[21], magnetic field[22], shear[23] and so on due to their large size (1-100 microns) and slow movement (milliseconds to seconds). The control of different types of colloidal crystal geometries can be of technological importance for the construction of certain devices, such as photonic band-gap materials. Understanding colloidal systems under external perturbations from microscopic considerations has drawn considerable research interests[24–30].

The liquid-solid transition in two dimensional systems of colloidal particles under the influence of external modulating potentials has recently attracted attention in experiments [31], theory [32] and computer simulations [33, 34]. Chowdhury, Ackerson and Clark [35] show a charge stabilized colloidal liquid system, confined between two glass plates to form a single 2D layer, when subjected to an one dimensional stationary laser modulation whose periodicity matches with the mean particle distance, the system freezes to form a triangular lattice with full two dimensional symmetry. This phenomenon is known as Light Induced Freezing (LIF). Moreover, Loudiyi and others [36] study the effect of an externally applied field on the microstructure of aqueous suspensions of charge stabilized polystyrene

spheres by direct observation. The microstructure is observed as a function of the input intensity and crossing angle of the two beams. It is found that both single and multilayered systems exhibit a transition to crystal-like order. It is also found that this crystal order was more pronounced at large input power and for a periodic external field commensurate with the lattice spacing for a final undistorted two dimensional hexagonal crystal structure. Modulated colloids[35] show nontrivial physical behaviour both in equilibrium and out of equilibrium such as laser induced freezing [37, 38] and re-entrant melting[39–44], dynamical heterogeneity [45], nontrivial dynamics in single file diffusion [46–49], and in non-equilibrium steady state conditions [50–52], non-Newtonian rheology [53] to name only a few. There has been yet no comprehensive report on the dynamics of the modulated liquid so far. In this thesis, we study the dynamical behaviour of a modulated colloidal liquid.

Experiment on a 2D binary colloidal system with particles of different sizes have been reported. A sinusoidal light field by interferring two laser beams is created. Observation of real time trajectory using video microscopy is done. After that the system has been subjected to a spatially periodic potential using an external modulation generated in a given direction by interfering laser beams[54]. This study tunes both the amplitude of the laser beam and the area fraction of the system and probe into particle arrangements. The wavelength of the modulation matches with the diameter of the bigger particles, and the modulation is stronger for them than the smaller particles. An increase in the external modulation amplitude making the arrangement of the large particles analogous to a modulated liquid[35] has been observed. The larger particles make this arrangement by caging the smaller onces in big clusters. The smaller particles arrange themselves in a triangular fashion inside those cages. The large particles are observed to remain ordered, whereas the lattice of small particles became disordered upon increasing the temperature. There has been no study yet on how an external modulation changes the phase behaviour and dynamics in a binary colloid. This leads us to study the phase behaviour and dynamics of a modulated binary colloid.

III. HETEROGENEOUS DYNAMICS OF A MODULATED COLLOIDAL SYSTEM

We probe the structure and dynamics of modulated mono-disperse colloidal film under spatially periodic one-dimensional external modulation. We consider a 2D box of colloidal particles of diameter of $100\mu m$. We then use Brownian Dynamics (BD) simulation method at room temperature where the discretized Langevin dynamics including white noise has been numerically integrated. The diameter of the particles matches with the wavelength of the external potential. Initially in absence of external potential, the particles from a homogeneous liquid like arrangement as observed from Fig. 1(a). We observe that the particles align themselves along the potential minima

in equilibrium. This alignment makes the system modulated along the direction of modulation as shown in Fig. 1(b). The snapshots (Fig. 1) suggest that system gets into modulated liquid phase in presence of the external potential. We characterize the dynamics in the system by the mean square displacements and the self-van Hove function. Computation of mean square displacement considers the displacement of the particle at time t, while self-van Hove function is the probablity distribution of those displacements. We find that diffusion coefficients, obtained from long time mean sqaure displacements, decay exponentially with increasing potential strength. The self-van Hove functions computed from the distribution of particle displacemets in a given time interval show non-gaussian behaviour in directions both parallel and transverse to the external modulation, unlike gaussian profile in normal liquid. This suggests heterogeneous dynamics and is supported by particle mobilities and residence times.

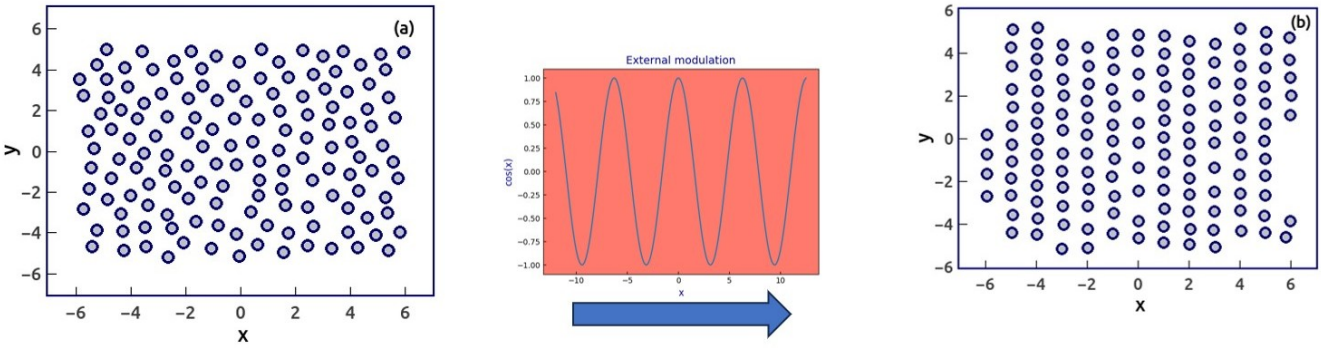

FIG. 1: Liquid to modulated liquid transition in presence of external modulation. Final configuration at (a) $\beta V_0 = 0.0$ and (b) $\beta V_0 = 10.0$.

IV. MIXING-DE-MIXING OF BINARY DEMIXED COLLOIDAL SYSTEM

We look into a binary system consisting of mutually repelling colloidal particles with different sizes under external modulation. We explore phase behaviour of a binary colloidal system under external spatially periodic modulation. We perform Monte Carlo simulation on a binary mixture of big and small repulsive particles with diameter ratio 2:1. We characterise structure by isotropic and anisotropic pair correlation function, cluster size distribution and bond angle distribution. We observe demixing of the species in absence of the external modulation due to strong cross-species interaction as shown in Fig. 2(a). The species gradually mix with one another which gets enhanced with increasing potential strength as shown in Fig. 2(b). We also compute the demixing order parameter and specific heat of the system. The de-mixing order parameter shows discontinuity with increasing modulation strength, characterizing

a first order phase transition. The peaks in specific heat and the order parameter jump increases with the size of the system. We examine the dynamical behaviour of the system via computing Mean Square Displacement (MSD) along both parallel and perpendicular direction to the modulation. We observe decrease in diffusion coefficient for both types of particles as we increase the strength of the modulation.

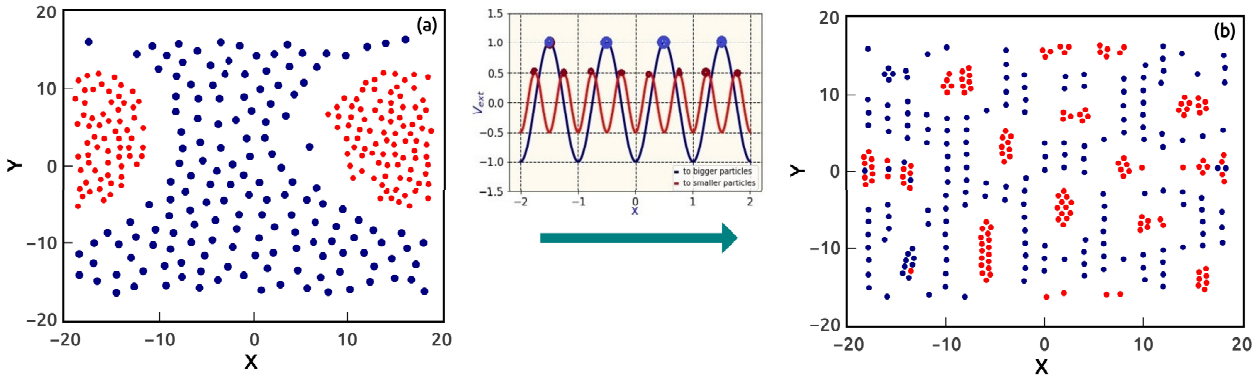

FIG. 2: Phase transition from demixed binary to mixed modulated binary mixture. Final configuration at (a) $\beta V_0 = 0.0$ and (b) $\beta V_0 = 10.0$.

Next we study the kinetics of formation of clusters of small particles after we turn off the external potential on the modulated binary colloidal mixture obtained previously. We start from initial mixed configuration (Fig. 3(a)) at high external modulation and then switch off the external modulation. We observe that the smaller particles gradually

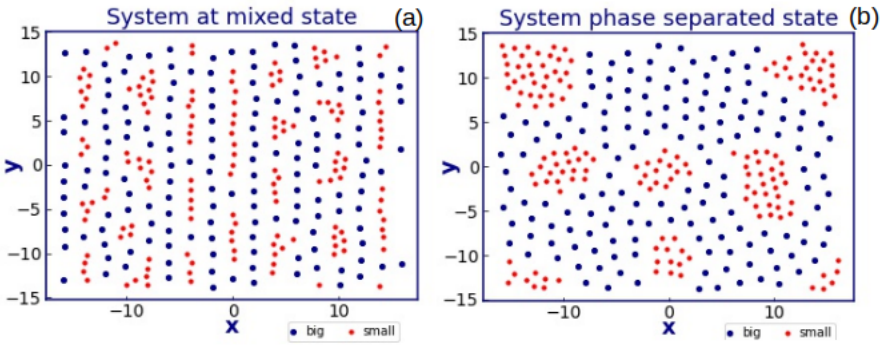

FIG. 3: Final configuration at (a) $\beta V_0 = 10.0$ and (b) $\beta V_0 = 0.0$.

keep forming big clusters (Fig. 3(b)) within pools of bigger particles. So the system goes from a mixed phase to a de-mixed phase with time. Cluster size analysis shows growth of sizes of clusters with time as a power law. The growth saturates as the system reaches equilibrium. We denote this time that the system takes to reach the new

equilibrium as transition time T_s. The diffusion coefficient show faster diffusion of bigger particles and slower diffusion of smaller particles with time in the transient state.

The thesis is organised as follows. We describe the simulation techniques and methods in chapter 2. Chapter 3 illustrates dynamical study on a mono-dispersieve colloidal system under external modulation. Chapter 4 demonstrates structural and dynamical properties of a demixed binary mixure under external modulating potential followed by chapter 5 were we report kinetical study on modulated mixed binary colloidal system. Chapter 6 concludes the thesis.

---

[1] C. Bechinger and E. Frey, J. Phys.: Condens. Matter **13**, R321 (2001).

[2] M. C. Jenkins and S. U. Egelhaaf, J. Phys.: Condens. Matter **20**, 404220 (2008).

[3] L. Radzihovsky, E. Frey and D. R. Nelson, Phys. Rev. E **63**, 031503 (2001).

[4] H. Löwen, J. Phys.: Condens. Matter **13**, R415 (2001).

[5] H. Löwen, Eur. Phys. J. ST **222**, 2727 (2013).

[6] Yethiraj, A., van Blaaderen, Nature **421**, 513517 (2003).

[7] Cho, Y. S. *et al.* J. Am. Chem. Soc. **127**, 1596815975 (2005).

[8] Lin, Y. S. *et al.* Chem. Mater. **17**, 45704573 (2005).

[9] Zoldesi, C. I. & Imhof, A. Adv. Mater. **17**, 924928 (2005).

[10] Garcia-Santamara, F. *et al.* Adv. Mater. **14**, 11441147 (2002).

[11] Vinothan N. Manoharan *et al.*, Science **301**, 483-487(2003).

[12] Y. Han and David G. Grier Phys. Rev. Lett. **9**1, 038302 (2003).

[13] I. Sriram and Eric M. Furst Soft Matter **8**, 3335-3341 (2012).

[14] W. K. Kegel, and A. van Blaaderen, Science **287**, 290-293 (2000).

[15] M.P. Allen, D.J. Tildesley Computer Simulation of Liquids, Clarendon Press, Oxford (1987)

[16] D. Frenkel and B. Smit, Understanding Molecular Simulation, Academic Press, San Diego (1996)

[17] A. Darras, E. Opsomer, N. Vandewalle *et al.* Eur. Phys. J. E **42**, 123 (2019).

[18] Yu. A. Buyevich and A. O. Ivanov Physica A: Statistical Mechanics and its Applications, **190**, 276-294, (1992).

[19] Per Linse, *Simulation of Charged Colloids in Solution*, Advanced Computer Simulation Approaches for Soft Matter Sciences II, **185** (2005).

[20] Q. H. Wei, C. Bechinger, D. Rudhardt and P. Leiderer, Phys. Rev. Lett. **81**, 2606 (1998).

[21] A. Kriisa and Connie B. Roth, ACS Macro Letters **8** 188-192 (2019).

[22] K. Zahn, R. Lenke and G. Maret, Phys. Rev. Lett. **13**, 2721 (1999).

[23] A. Zaccone, H. Wu, D. Gentili and M. Morbidelli, Phys. Rev. E **80**, 051404 (2009).

[24] D W Jepsen, J. Math. Phys. **6 405** (1965).

[25] K. Hahn and J. Kärger, J. Phys. Chem. B **102** 5766 (1998).

[26] Kollmann, Phys. Rev. Lett. **90**, 180602 (2003).

[27] B. Delfau, C. Coste and M. S. Jean Phys.Rev. E **84** 011101 (2011).

[28] A. Einstein *Investigations on the Theory of The Brownian Movement* ed R Fürth (USA, Dover Publications, INC.) (1956).

[29] Frey E and Kroy K 2005 *Ann. Phys.* **14** 20

[30] Coupier G, Jean M S and Guthmann C 2006 *Phys. Rev.* E **73** 031112.

[31] Q.-H. Wei, C. Bechinger, D. Rudhardt and P. Leiderer, Phys. Rev. Lett. **81**, 2606 (1998).

[32] E. Frey, D. R. Nelson, L. Radzihovsky, Phys. Rev. Lett. 83, 2977 (1999)

[33] K. Loudiyi, B. J. Ackerson, Physica A **184**, 1 (1992); pages 26-41 (1992)

[34] C Das, Pinaki Chaudhuri, AK Sood, HR Krishnamurthy inCurrent science **80(8)** April 2001

[35] A. Chowdhury, B.J. Ackerson, N. A. Clark, Phys. Rev. Lett. **55**, 833 (1985).

[36] K. Loudiyi, B. J. Ackerson, Physica A **184**, 1 (1992); pages 1-25 (1992)

[37] K. Loudiyi, B. J. Ackerson, Physica A **184**, 1 (1992).

[38] J. Chakrabarti, H.R. Krishnamurthy, A. K. Sood, Phys. Rev. Lett. **73**, 2923 (1994)

[39] J. Chakrabarti, H. R. Krishnamurthy, A. K. Sood and S. Sengupta, Phys. Rev. Lett. **75**, 2232 (1995).

[40] C. Bechinger, M. Brunner and P. Leiderer, Phys. Rev. Lett. **86**, 930 (2001).

[41] E. Frey and K. Kroy K, Ann. Phys. **14**, 20 (2005).

[42] E. Frey, D. R. Nelson and L. Radzihovsky, Phys. Rev. Lett. **83**, 2977 (1999).

[43] M. Schmiedeberg, J. Roth and H. Stark H, Phys. Rev. Lett. **97**, 158304 (2006).

[44] S. Deutschländer, T. Horn, H. Löwen, G. Maret and P. Keim, Phys. Rev. Lett. **111**, 098301 (2013).

[45] W. K. Kegel and A. van Blaaderen, Science **287**, 290 (2000).

[46] K. Hahn and J. Kärger, J. Phys. Chem. B **102**, 5766 (1998).

[47] M. Kollmann, Phys. Rev. Lett. **90**, 180602 (2003).

[48] B. Delfau, C. Coste and M. S. Jean, Phys.Rev. E **84**, 011101 (2011).

[49] G. Coupier, M. S. Jean and C. Guthmann, Phys. Rev. E **73**, 031112 (2006).

[50] T. Speck *et. al.* EPL **79**, 30002 (2007).

[51] A. Würger, Rep. Prog. Phys. **73**, 126601 (2010).

[52] Xiao-guang Ma, *et. al.* Phys. Rev. E **91**, 042306 (2015).

[53] J. Bergenholtz, J. F. Brady and M. Vicic, Journal of Fluid Mechanics **456**, 239-275 (2002).

[54] R. F. Capellmann, A. Khisameeva, F. Platten and S. U. Egelhaaf, J. Chem. Phys. **148** 114903 (2018).

Chapter 2: Methods

In this thesis I use two different simulation techniques to study phase and dynamics of a system of modulated colloids, namely, Brownian Dynamics and Monte Carlo simulations. I discuss below the salient features of these two techniques. Brownian dynamics simulations is described in section I and the Monte Carlo simulations in section II.

I. BROWNIAN DYNAMICS SIMULATION

Brownian motion is exhibited by colloidal particles suspended in a fluid. The randomness of movement comes from collision with fast moving solvent molecules. The motion is described by stochastic differential equation unlike deterministic Newtonian equation of motion.

A. Langevin equation of motion for single particle

The Langevin equation of motion[1] to describe random motion of a colloidal particle of mass m, and velocity $\mathbf{u}(t)$ in a bath of much smaller particles is given by:

$$m\dot{\mathbf{u}}(t) = -m\gamma\mathbf{u}(t) + \mathbf{R}. \tag{1}$$

where $\gamma = 6\pi\eta d$ is the friction coefficient of the solvent bath with d being the diameter of the colloidal paricle η the viscosity coefficient of the solvent. The random forces $\mathbf{R}$ on the particles are due to random bombardment of the solvent particles. This random force has mean:

$$\langle \mathbf{R}(t) \rangle = 0 \tag{2}$$

and has infinitesimally short correlation time:

$$\langle \mathbf{R}(t+s).\mathbf{R}(s)\rangle = 2\pi R_0 \delta(t-s) \tag{3}$$

The two terms on the right hand side of eq. (1) are not independent of each other which can be demonstrated as follows. The formal solution to Eq. (1) is:

$$m\mathbf{u}(t) = m\mathbf{u}(0)e^{-\gamma t} + e^{-\gamma t}\int_0^t e^{\gamma s}\mathbf{R}(s)ds \tag{4}$$

On squaring and taking statistical average over noise we get,

$$\begin{aligned} m^2\langle|\mathbf{u}(t)|^2\rangle \quad &= \quad m^2\langle|\mathbf{u}(t)|^2\rangle e^{-2\gamma t} + e^{-2\gamma t}\int_0^t ds\int_0^t e^{\gamma(s+s')}2\pi R_0\delta(s-s') \\ &= m^2\langle|\mathbf{u}(t)|^2\rangle e^{-2\gamma t} + \frac{\pi R_0}{\gamma}[1-e^{-2\gamma t}] \end{aligned} \tag{5}$$

In large time limit, we get : $\langle|\mathbf{u}(\propto)|^2\rangle = \frac{\pi R_0}{\gamma}$. Now, the necessary condition for the particle to be in equilibrium with the bath at large time is: $\langle|\mathbf{u}(\propto)|^2\rangle = 3K_BT/m$ as given by the equi-partition theorem. Thus, in the thermal equilibrium,

$$\gamma = \frac{\pi R_0}{3mK_BT} = \frac{1}{3mK_BT}\int_0^{\propto}\langle\mathbf{R}(t).\mathbf{R}\langle dt \tag{6}$$

γ can also be related to the diffusion coefficient of the particle. Let us consider that the particle is at origin ($\mathbf{r}=0$) at initial time $t=0$. Now, multiplying Eq.(1) by $\mathbf{r}(t)$ we get,

$$\mathbf{r}.\mathbf{u} = \mathbf{r}.\dot{\mathbf{r}} = \frac{1}{2}\frac{d}{dt}r^2, \qquad \mathbf{r}.\dot{\mathbf{u}} = \mathbf{r}.\ddot{\mathbf{r}} = \frac{1}{2}\frac{d^2}{dt^2}r^2 - u^2 \tag{7}$$

Using this we get,

$$\frac{1}{2}m\frac{d^2}{dt^2}|\mathbf{r}(t)|^2 + \frac{1}{2}\gamma m\frac{d}{dt}|\mathbf{r}(t)|^2 = m|\mathbf{u}(t)|^2 + \mathbf{r}(t).\mathbf{R}(t) \tag{8}$$

Now, taking average over noise, we get:

$$\frac{d^2}{dt^2}\langle|\mathbf{r}(t)|^2\rangle + \gamma\frac{d}{dt}\langle|\mathbf{r}(t)|^2\rangle = \frac{6K_BT}{m} \tag{9}$$

Further, using the boundary conditions: $\frac{d}{dt}\langle|\mathbf{r}(t)|^2|\rangle_{t=0} = 2\langle\mathbf{r}(0).\mathbf{u}(0)\rangle = 0$, we get:

$$\langle|\mathbf{r}(t)|^2\rangle = \frac{6K_BT}{\gamma m}(t - \frac{1}{\gamma} + \frac{1}{\gamma})e^{-\gamma t} \tag{10}$$

, At very large time ($\gamma t >> 1$) the equation reduces to:

$$\langle|\mathbf{r}(t)|^2\rangle = \frac{6K_BT}{\gamma m}t \tag{11}$$

which leads to Einstein's equation for diffusion constant: $D = \frac{K_BT}{\gamma m}$

B. Brownian Motion in the Over damped limit

Let us consider a small change in velocity $\Delta\mathbf{u} = \mathbf{u}(t) - \mathbf{u}(0)$ in Eq.1. Taking average over noise we get:

$$m\langle\Delta\dot{\mathbf{u}}\rangle = -m\gamma\langle\mathbf{u}\rangle \tag{12}$$

The solution is: $\Delta u \propto exp(-\frac{\gamma}{m}t)$. Here m/γ is the velocity relaxation time. The change in velocity relaxes within this time. The relaxation time is sufficiently small in case of very high damping ($\gamma- >\propto$). In such cases, one can ignore the inertial term. This is called the over-damped limit of Langevin equation as given below:

$$m\gamma\mathbf{u}(t) = \mathbf{R} \tag{13}$$

In the presence of many Brownian particles, we take into account of the systematic forces arising due to colloidal interaction. The equation becomes after discretization[2] over time is:

$$\mathbf{r}_i(t + \Delta t) = \mathbf{r}_i(t) + \frac{\Delta t}{\gamma}(\mathbf{F}_i^{int} + \mathbf{F}_i^{ext}) + \mathbf{R}_i(t), \tag{14}$$

where $\mathbf{r}_i(t)$ is the position of i^{th} particle at time t and Δt the time interval for integration. $\mathbf{F}_i^{int} = -\nabla_i\Sigma_{ij}V(r_{ij})$ is the force due to pair interaction $V(r_{ij})$ between the colloidal particles

and the force due to the external potential is:

$$\mathbf{F}_i^{ext}(\mathbf{r}_i) = -\nabla_i V_{ext}(\mathbf{r}_i) \tag{15}$$

Now, let us cnsider $\mathbf{R}_i(t)$ to be random displacement having Gaussian statistics with $\langle \mathbf{R}_i(t) \rangle = 0$; $\langle \mathbf{R}_i(t)\mathbf{R}_i(t') \rangle = 2D\delta(t-t')$. We generate the Gaussian random numbers using the Box-Muller transformation[3, 4] on two uniform random numbers R_1 and R_2 between 0 and 1 as shown in Fig. 1. Since they fall within the circle as described in Fig. 1, $s = R^2 (= R_1^2 + R_2^2)$ which is the area divided by π also falls within [0,1] and θ falls within $[-\pi, \pi]$.

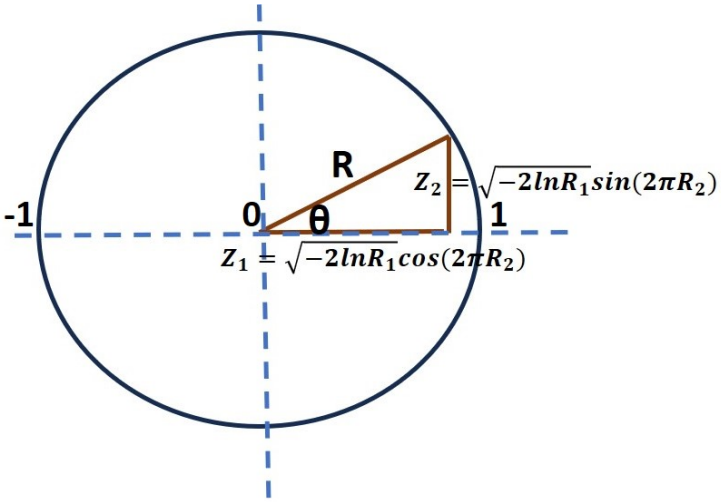

FIG. 1: Box-Muller transformation.

We also know that the norm of a bi-variate normal distribution is $s = -2lnR_1$ and we can write θ as $\theta = 2\pi R_2$. Thus we generate Gaussian random numbers Z_1 and Z_2 from the uniform random numbers R_1 and R_2 in the range [0,1] applying the transformation:

$$Z_1 = (-2lnR_1)^{-1/2} cos(2\pi R_2) \;\; and \;\; Z_2 = (-2lnR_1)^{-1/2} sin(2\pi R_2) \tag{16}$$

Each particle is moved according to systematic force, external force and random Gaussian movements. Thus Brownian Dynamics simulation generates stochastic Brownian trajectory

of all the particles in constant NVT or canonical ensemble. Due to stochastic nature of trajectories, any quantity calculated using the trajectory are averaged over different realization of noise and different initial configurations.

II. MONTE CARLO SIMULATION

Monte Carlo simulation[1] is powerful technique to explore the phase space of a system stochastically as detailed below.

I first generate a two dimensional simulation box with a total of N numbers of particles arranged in a triangular lattice formation. Let us consider a point configuration in space of N numbers of particles with positions $\mathbf{r}_1, \mathbf{r}_2, ...\mathbf{r}_i, .., \mathbf{r}_N$ and potential energy $\mathcal{U}(\mathbf{r}_1, \mathbf{r}_2, ...\mathbf{r}_i, .., \mathbf{r}_N)$. Then I choose a random particle i and displace it randomly as $\mathbf{r}_i \hookrightarrow \mathbf{r}_i' = \mathbf{r}_i + \delta\mathbf{r}$ where $\delta\mathbf{r}$ is the random displacement in any arbitrary direction over a sphere of radius $\delta\mathbf{r}_{max}$. The new potential energy due to this move becomes $\mathcal{U}(\mathbf{r}_1, \mathbf{r}_2, ...\mathbf{r}_i', .., \mathbf{r}_N)$. Now the change in potential energy before and after the move is given by :

$$\delta\mathcal{U} = (\mathcal{U}(\mathbf{r}_1, \mathbf{r}_2, ...\mathbf{r}_i, .., \mathbf{r}_N) - \mathcal{U}(\mathbf{r}_1, \mathbf{r}_2, ...\mathbf{r}_i', .., \mathbf{r}_N)) \tag{17}$$

If $\delta\mathcal{U} < 0$, then that MC move is accepted. This is because the system always tries to attain minimum energy, hence decrease in energy is always favourable. But if that is not the case,

I generate a uniform random number say Z in the range 0 to 1. According to the Metropolis algorithm, if this ratio $\exp(-\beta\mathcal{U}) > Z$, then the MC move is accepted. Thus the acceptance rule for Monte Carlo sampling is summarised as:

$$P_{acc} = min[1, exp(-\beta\delta\mathcal{U}) \tag{18}$$

Thus I set up a canonical or constant-NVT ensemble of states of the liquid, choosing individual states with the appropriate probability, and calculating the configurational energy by

averaging uniformly over the ensemble.

This simulation samples a region of phase space in order to estimate certain properties of the system, which may not be a solution to the equation of motion of the system. Hence, the MC simulation can not yield dynamical information. However, the ensemble average can be computed with high degree of precision. The primary step in the simulation is to generate new co-ordinates of the particles starting from some initial configuration in phase space.

Let us consider any microscopic variable A. The expectation value of A taking the canonical ensemble average is:

$$\langle \mathcal{A} \rangle_{NVT} = \langle \mathcal{A} \rho_{NVT} \rangle = \frac{\int d\mathbf{r}\ \mathcal{A}\ exp(-\beta \mathcal{U})}{\int d\mathbf{r}\ exp(-\beta \mathcal{U})} \tag{19}$$

It is observed from the above equation that the expectation value highly depends upon the Boltzmann factor. So the simulation chooses random points from the distribution only in the region of space where important contributions to the integral are made by the evaluation of the distribution function. This is known as importance sampling.

III. THERMODYNAMIC LIMIT

BD and MC Simulation methods are used to study a model system numerically. Any simulation uses boxes with finite numbers of particles. In order to compare to size of experimental systems, these boxes need to be infinite. In a finite box, there are surface effects due to the boundary which are not present in the bulk system.

This problem with surface effects is resolved using periodic boundary conditions (PBCs)[1]. The simulation box is replicated in space as can be seen in Fig. 2 for a 2D

system for illustration. The particles within the replicas are called the images of the particles of the central box. In the figure, the replica of the original boxes are marked as A, B, C etc and the original one is marked as O. The images of the original particles move accordingly with those in the central box.

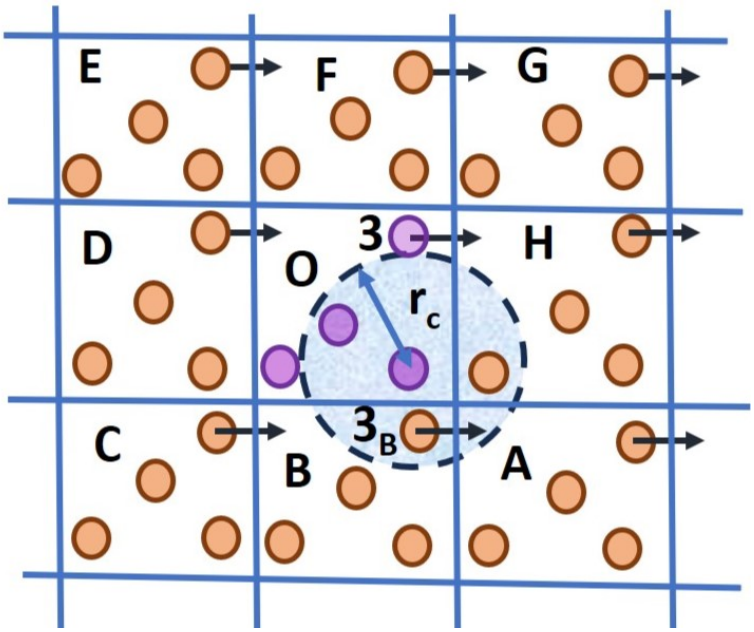

FIG. 2: Particles move out of the central box, and one of its images enter within. The interactions are considered for only those ones lying within r_c.

While translating the particles in the box, if a particle moves out of the original box, then one of its images from the adjacent boxes comes back to the central box. We can see in Fig. 2 that as the 3^{rd} particle in the central box moves out of it, one of its image from box D moves within it, keeping the total number of the particles fixed in all the boxes. Thus, the particles do not experience the boundary.

The calculations of energy and the total force on a particular particle involves the interactions with the rest $N-1$ numbers of particles and all the particles in the image boxes. This makes the computations expensive and scaling of the computation cost like N^2. One

can reduce the computational cost by considering the particles including those in the image boxes within a sphere of a cut-off radius r_c surrounding a given particle (say O in Fig. 2). One takes into account the minimum of the pair-distances considering the central particle O and the other particles in the circle if the potential is short ranged. This is called the minimum image convention (MIC)[1]. In Fig. 2, the distance between particle 1 and image of particle 3, 3_B is taken into account instead of the original particle 3. This is because the distance to the image is shorter than the original one.

It is important to note that while PBC is a powerful technique, it introduces some limitations, such as the inability to model large-scale spatial fluctuations and the cases of long-range correlations.

---

[1] Hansen J P, McDonalds I R *Theory of simple liquids* (UK, Elsevier Academic Press) (1986).

[2] D. L. Ermak and Y. Yeh, J. Chem. Phys. **62**, 4189 (1975).

[3] William H. Press, Saul A. Teukolsky, William T. Vetterling and Brian P. Flannery, *Numerical Recipes in Fortran 77: The Art of Scientific Computing* (Cambridge University Press, New York, 2nd. eds., 1992)

[4] Luc Devroye, *Non-Uniform Random Variate Generation* (New York: Springer-Verlag, 1986)

Chapter 3: Dynamics of a periodically modulated colloidal liquid*

I. INTRODUCTION

In this chapter I illustrate the dynamics, of modulated liquid phase of colloids. Several years ago Chowdhury, Ackerson and Clark subjected a charge stabilized colloidal liquid system, confined between two glass plates to a one-dimensional stationary laser modulation whose periodicity matches with the mean particle distance[1]. For low field the system shows density modulation parallel to the external potential. However, the particles along the minima of the external potential show liquid like order resulting in a modulated liquid phase. The modulated liquid phase freezes to form a triangular lattice with full two dimensional symmetry[1, 2] for sufficiently large modulation strengths. This has been confirmed by density functional theory (DFT)[3]. In this study transition from modulated liquid phase to crystalline phase with increase in the strength of modulating potential has been reported. MC simulation shows that the system freezes first due to the increase in the strength of the potential, but after a certain field strength the system returns back to modulated liquid phase[4]. Reentrant modulated liquid phase has been experimentally verified subsequently[5]. This unusual behaviour is investigated in the light of Kosterlitz, Thouless, Halperin, Nelson, and Young (KTHNY) theory[6, 7]. There have been variety of studies on colloids under external potential which include freezing and melting of a colloidal adsorbate on a one dimensional quasi crystalline substrate[8], two-dimensional melting behaviour of super paramagnetic colloidal particles under quenched disorder[9], effective forces in modulated colloids[10], modulated phases in dense [11] and binary colloids[12] to name only a few. Experiments and simulations on colloidal suspensions under external potentials have been reviewed in recent years[13–15].

The dynamics of modulated colloid is yet to be explored in details. Brownian Dynamics simulations on periodically modulated colloids showed that mean square displacements(MSD) along both parallel and perpendicular to modulation direction have sub-diffusive region[16] similar to super cooled systems. However, the MSDs alone do not characterize the particle motion. The probability distribution of particle displacements in a given time interval, known as the self-van Hove function (self-vHf) which can be probed by neutron scattering measurements, gives full information on particle motion[17]. The MSD is the second moment of the self-vHf. In a normal liquid, the self-vHf is gaussian[17]. But super cooled liquids[18–22], glassy systems[23], systems close to jamming transitions[24–28], non-equilibrium

---

* Suravi Pal and J Chakrabarti, J. Phys.: Condens. Matter **32** 124001 (2020).

steady states of granular gases, plasma and lane forming colloids [29–36] all show non-gaussian self-vHf. The non-gaussian self-vHf is phenomenologically interpreted in terms of dynamic heterogeneity where regions of different diffusion coefficient co-exist in the system[37]. Later experiments [38] have probed MSD and self-vHf for modulated colloids in extreme dilute limit, restricting only to the modulation direction. The experiments show sub-diffusive MSD and non-gaussian self-vHf in presence of both periodic and random external potential[39].

The colloidal particles tend to accumulate around the minima of the modulation potential that leads to transverse motions coupled to those in the modulation direction. Thus, the full dynamical characterization can be done by considering particle motions both in the parallel and transverse directions. Here I probe dynamics of a periodically modulated colloid both along parallel and transverse to the modulation direction by means of MSD and self-vHf. my aim is to understand the complete dynamical feature and their tunability by the external modulation. I perform Brownian Dynamics (BD) simulation, as described in Chapter II, for a colloidal film subjected to a one dimensional periodic modulation with wavelength equal to mean inter-particle separation as in Refs.[38, 39] . The colloidal particles in my system interact with each other via electrostatic screened repulsion potential[40]. The diffusion coefficients, estimated from long time MSDs, decreases exponentially with external modulation strength both along the modulation and the transverse directions. The self-vHfs in both the directions show non-gaussian behaviour, suggesting dynamical heterogeneity in the system. Tracking the individual motions supports the coexistance of particles with different mobilities in the system. The heterogeneity in dynamics is also supported by large variations in residence times of the particles.

This chapter is organised as follows: I describe the system details and methods used in Section II. Section III describes my observations in structural properties, Section IV the dynamical properties. I finally summarise my key findings and outlook of my work in Section V.

II. SYSTEM AND METHOD

I perform BD simulation using the discretised Langevin equation in overdamped limit as explained in chapter II:

$$\vec{r_i}(t+\Delta t) = \vec{r_i}(t) + \frac{\Delta t}{\gamma}(\vec{F_i}^{int} + \vec{F_i}^{ext}) + \vec{R_i}(t), \tag{1}$$

where $\vec{r_i}(t)$ is the position of i^{th} particle at time t, Δt the time interval for integration, and $\gamma(= 6\pi\eta d)$ the damping factor, d the diameter of the particle and η the visocity coefficient. $\vec{F_i}^{int}$ is the force due to pair interaction $V(r_{ij})$

between the colloidal particles at $\vec{r_i}$ and $\vec{r_j}$ with seperation $r_{ij} = |\vec{r_i} - \vec{r_j}|$ given by the DLVO form[39]:

$$V(r_{ij}) = \frac{(Z^*e)^2}{\epsilon}(\frac{exp(\kappa d)}{(1+\kappa d)})^2 \frac{exp(-\kappa r_{ij})}{r_{ij}}, \tag{2}$$

where $1/\kappa$ is the Debye screening length, Z^* the effective surface charge on the colloidal particles, ϵ the dielectric constant of the medium and e the fundamental electronic charge. $\vec{F_i}^{ext}$ is the force due to the external modulating potential in x-direction of the form of

$$V_{ext}(x_i) = -V_0 cos(\frac{2\pi x_i}{a_s}), \tag{3}$$

where a_s is the wavelength of the external potential matching with the mean inter-particle seperation, and V_0 the strength of the external potential. $\vec{R_i}(t)$ is random displacement having Gaussian statistics with $\langle \vec{R_i}(t) \rangle = 0$; $\langle \vec{R_i}(t)\vec{R_i}(t') \rangle = 2D_0\delta(t-t')$ where $D_0 (= k_BT/6\pi\eta d)$ is the Einstein-Stokes diffusion coefficient at solvent temperature T, k_B being the Boltzman constant.

I take a_s as the length unit; $\tau_B (= d^2/D_0)$, the time taken by the particles to diffuse through their own diameter as the time unit and k_BT as the energy unit. I take an aqueous suspension ($\eta = 1cP$) of colloidal system of $N = 900$ particles of diameter ($d =$)$1\mu m$ in a rectangular box of length in x-direction, $l_x/a_s = 30.0$, and length in y-direction $l_y = \frac{\sqrt{3}}{2} l_x$ with the PBCs as mentioned in Chapter II. I take $Z^* = 7800$, $\varepsilon = 80$, $\rho d^2 = 1.0$ and $\kappa a_s = 10.0$. I also take r_{cut} to be the cut-off radius in the simulation box to ensure MIC as described in chapter 2. The integration time step is taken to be $\Delta t = 0.0001\tau_B$. I generate $N_i (= 15)$ Brownian trajectories starting from different equilibrium configurations upto $20\tau_B$.

I characterize structure by static density distribution $\rho(x, y)$ in xy plane. I bin the particle positions with bin width 0.06 in the centre of mass frame. I calculate MSDs of the particles along both x and y-directions from their displacements in successive time intervals starting from an initial time t_0 :

$$\langle (\Delta x)^2 \rangle = \langle \frac{1}{N} \Sigma_i (x(t) - x(t_0))^2 \rangle \tag{4}$$

and

$$\langle (\Delta y)^2 \rangle = \langle \frac{1}{N} \Sigma_i (y(t) - y(t_0))^2 \rangle. \tag{5}$$

The average is taken over $N_T (= 20)$ different initial times t_0 chosen over a Brownian trajectory. I then take average over different Brownian trajectories ($N_T = 15$) using the MSD plots and compute the slopes at longer times to get the diffusion coefficient of colloidal particles along both the axes.

I further compute self-van Hove function $G_s(\Delta\vec{r}, \Delta t)$ defined as:

$$G_s(\Delta\vec{r}, \Delta t) = \langle \frac{1}{N} \Sigma_{i=1}^{N} \delta[\vec{r} - \vec{r}_i(t) + \vec{r}_i(0)] \rangle. \tag{6}$$

I calculate $G_s(\Delta x, \Delta t)$ and $G_s(\Delta y, \Delta t)$ from the displacements of particles in a given time interval separately both along parallel and transverse to the modulation directions.

III. STRUCTURAL PROPERTIES

I carry out Brownian Dynamics simulations using Eq.1 with interaction potential given in Eq.2 and in presence of external potential in Eq.3. The equilibriation of the system is monitored by the total potential energy. I study the structural properties in terms of the density profiles. The dynamical properties are characterized in terms of the MSD (Eqs. 4 and 5), self-vHf (Eq.6) and the residence time of the particles in the system for different strength (βV_0) of the modulation potential.

First, I consider the structure of the system in equilibrium. I plot the final configuration after equilibrium has reached in Fig. 1(a). I also characterize structure by static density distribution $\rho(x, y)$ in xy plane. I bin the particle positions with bin width 0.06 in the centre of mass frame. I show a bulk ($\beta V_0 = 0.0$) liquid density profile in Fig.1(b) in absence of any external modulation. Both the equilibrium configuration (Fig. 1(a)) and density contour

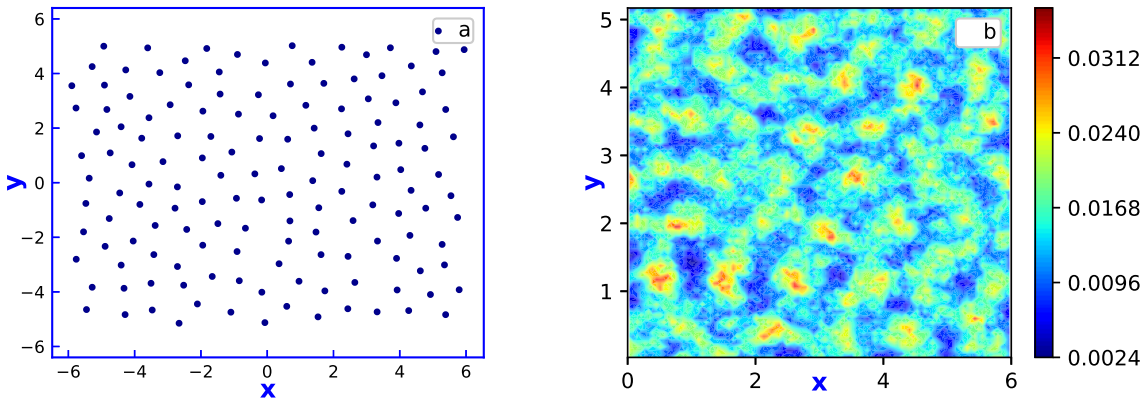

FIG. 1: (a) configuration and (b) density contour plot at $\beta V_0 = 0.0$.

plot (Fig. 1(b)) that in absence of any external modulation, the particles were arranged homogeneously in phase space.

Now, let us consider the system after being subjected to an external modulation. I show in Fig. 2(a) density profile

along x in the presence of external potential for $\beta V_0 = 1.0$ (black solid line) and $\beta V_0 = 10.0$ (gray solid line). $\rho(x)$ shows high density of particles at the minima of the external potential. The peaks get sharper and the width becomes narrower with increase in potential strength, indicating stronger modulation in system along x-axis. The average value of the density peaks, ρ_{max}, plotted against βV_0 in Fig. 2(b), shows initial increase and then saturation beyond $\beta V_0 = 10.0$. The saturation indicates that the accumulation of the particles over the minima locations are complete. There is hardly any particle off the minima locations. Inset in Fig. 2(b) exhibits $\rho(y)$ versus y. The density shows only a small variation, indicating uniformity in the transverse direction. Thus a modulated liquid phase has been generated in agreement to previous observation[3, 4, 41].

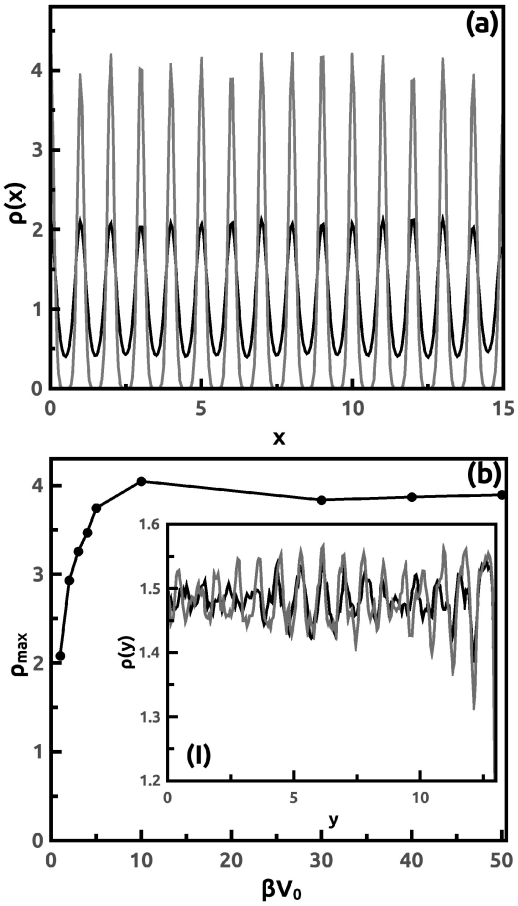

FIG. 2: $\rho(x)$ vs. x plots for (a) $\beta V_0 = 1.0$ (black line) and $\beta V_0 = 10.0$ (gray line). (b) ρ_{max} vs. βV_0 plot. Inset: $\rho(y)$ vs. y for $\beta V_0 = 1.0$ (black line), $\beta V_0 = 10.0$ (gray line).

I also characterise the structural correlations from the histograms of the separation between particle pairs, also called the radial distribution function (rdf) $g_(r)$. This quantity describes the probability of finding a pair of particles at separation r. I bin the separation between the particles with bin width 0.05 and compute its histogram. Fig. 3(a)

shows the rdf for the system in absence of external potential. $g(r)$ shows short ranged liquid structure with only a few peaks. The anisotropic structure of the system in presence of external potential is characterized by the pair anisotropic correlation functions (PCF) as shown in Fig. 3(b) denoted by $g(x, y)$. This is obtained by binning the pair separations both in x- and y-directions. When I apply modulation, $g(x, y)$ (Fig.3(b)) shows parallel strips along potential minima. This further confirms preferred particle positions at the modulation minima.

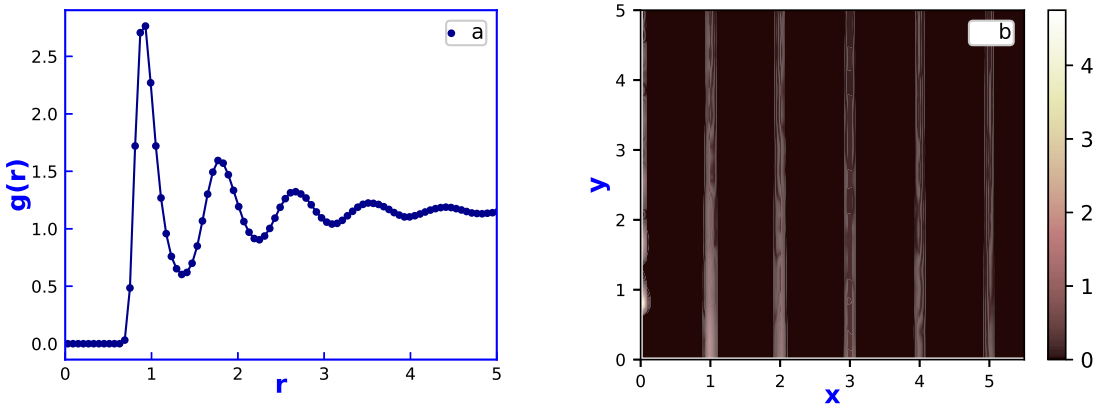

FIG. 3: (a) Radial distribution function $g(r)$ vs. r in absence of external potential, (b) anisotropic PCF when an external modulation has been applied in x-direction.

IV. DYNAMIC PROPERTIES

The MSDs $\langle(\Delta x)^2\rangle$ and $\langle(\Delta y)^2\rangle$ are plotted against time, t in log-log plot in Fig. 4. Fig. 4(a) shows $\langle(\Delta x)^2\rangle$ for $\beta V_0 = 1.0$ and 10.0. I observe slightly different slopes for small and large times, although both are close to unity for $\beta V_0 = 1.0$. $\langle(\Delta x)^2\rangle$ shows saturation with time for $\beta V_0 = 10.0$. Fig. 4(b) shows $\langle(\Delta y)^2\rangle$ for $\beta V_0 = 1.0$ and 10.0. For $\beta V_0 = 1.0$, the short time and long time slopes are different in this case as well. The long time slope is close to unity which confirms long time linear $\langle(\Delta y)^2\rangle$. For $\beta V_0 = 10.0$ I find sub-linear $\langle(\Delta y)^2\rangle$ with exponents 0.6 and 0.7 in the short and long times respectively. This dependence indicates sub-diffusive motion, also observed in single file diffusion[42–44]. I find that the motion along the perpendicular direction is also affected by the constrained motion along modulation direction. This is due to enhanced particle accumulation over the minima of the external potential with increasing modulation strength. MSDs deviating from linear time dependence were reported in earlier simulations[16] and experimental works[38, 39].

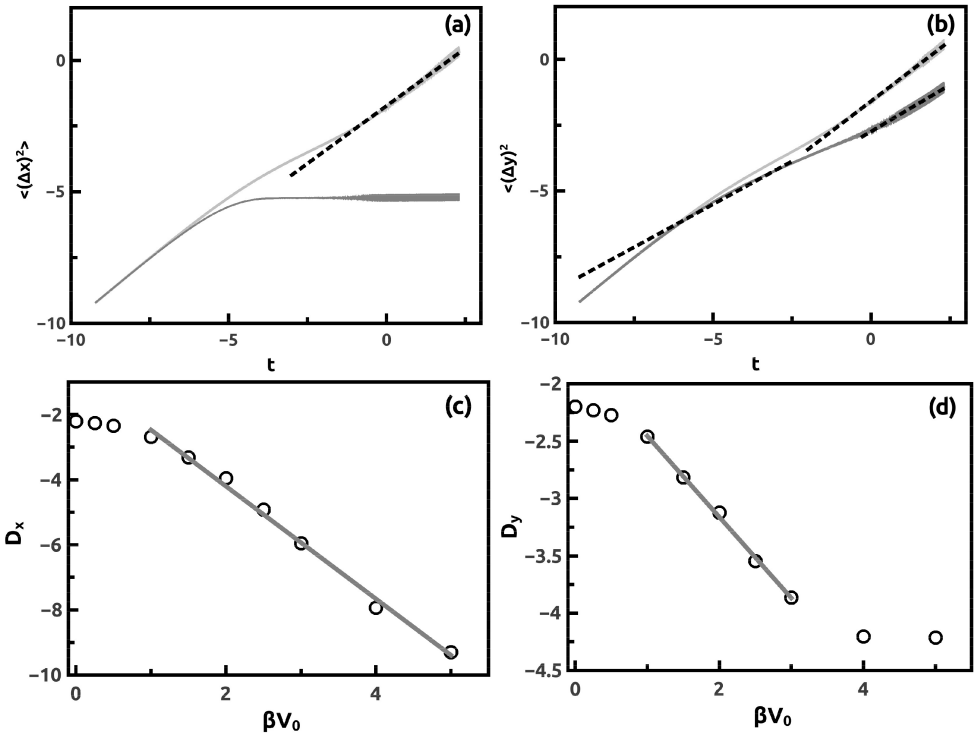

FIG. 4: (a) Log-log plot of mean-square displacement along x, $\langle(\Delta x)^2\rangle$ vs. time, t plot for $\beta V_0 = 1.0$ (light gray line), $\beta V_0 = 10.0$ (dark gray line). (b) Log-log plot of mean-square displacement along y, $\langle(\Delta y)^2\rangle$ vs. time, t plot for $\beta V_0 = 1.0$ (light gray line), $\beta V_0 = 10.0$ (dark gray line). Black dashed lines are the fitted lines at different times. (c) Semilog plot of diffusion co-efficient, D_x vs. βV_0 plot. (d) Semilog plot of diffusion co-efficient, D_y vs. βV_0 plot. Circles represent the simulated data. The solid lines are fitted curves.

I compute D_x and D_y from slopes of $\langle(\Delta x)^2\rangle$ and $\langle(\Delta y)^2\rangle$ versus t plots for linearly dependent MSDs as mentioned in Eq. (4) and (5). Fig. 4(c) shows the variation of D_x with βV_0 in semilog plot. I observe that initially D_x shows slow variation upto $\beta V_0 = 1.0$. Beyond $\beta V_0 = 1.0$, it falls rapidly following an exponential decay dependence as $D_x = A_x \exp^{-\alpha_x(\beta V_0)}$ with $A_x = 0.1353$ and $\alpha_x = 1.04$. At sufficiently high βV_0, for example at 10.0, I can not define D_x due to saturation of $\langle(\Delta x)^2\rangle$ at high βV_0. I plot variation of D_y with βV_0 in semilog plots in Fig. 4(d). I observe that D_x and D_y have identical values in absence of the external potential. D_y too, varies slowly in the region lower than $\beta V_0 = 1.0$ because of slow initial diffusion. Then it falls quite rapidly beyond $\beta V_0 = 1.0$ following exponential fall with βV_0 shown by linear fitting curves in the semi-log plots. The fitted dependence is as follows: ; $D_y = A_y \exp^{-\alpha_y(\beta V_0)}$ with $A_y = 0.1253$ and $\alpha_y = 0.49736$. I observe saturation of D_y beyond $\beta V_0 = 4.0$. The dynamics is sub-diffusive for $\beta V_0 > 5.0$. Experimental data in Ref.[38] is supportive of exponential dependence of diffusion coefficient on modulation strength in the modulation direction. The diffusion along the modulation direction is governed by escape

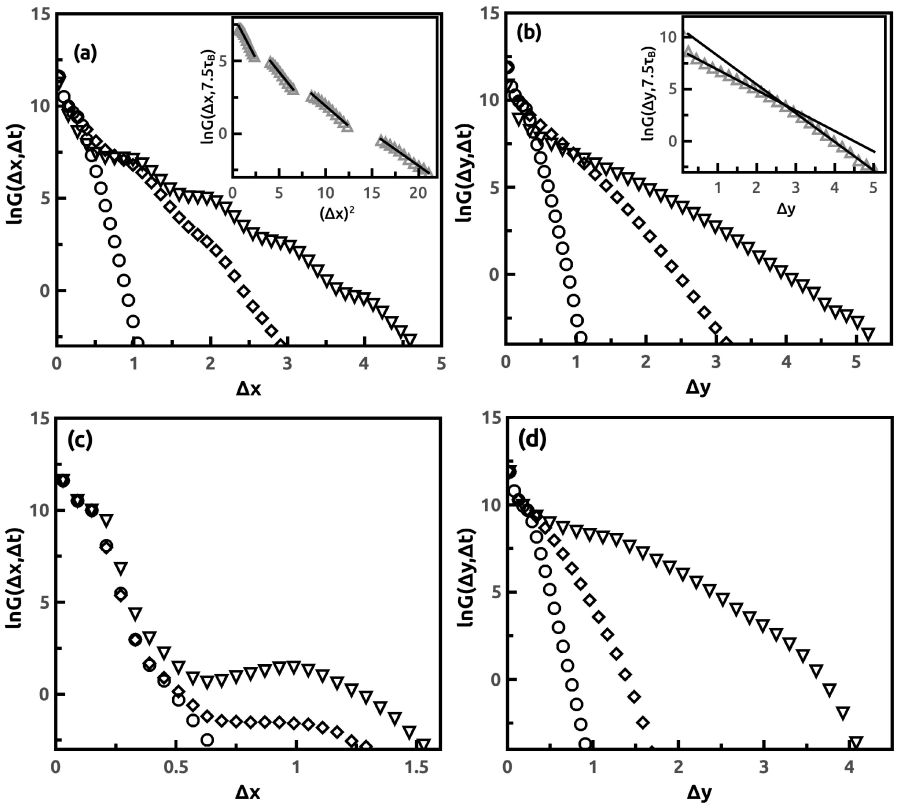

FIG. 5: (a) $lnG(\Delta x, \Delta t)$ vs. Δx with $\Delta t = 0.1\tau_B$ (circles), $\Delta t = 2.0\tau_B$ (squares), $\Delta t = 7.5\tau_B$ (triangles) for $\beta V_0 = 1.0$; Inset: linear fitting of $lnG(\Delta x, 7.5\tau_B)$ vs. $(\Delta x)^2$ corresponding to different peaks in $lnG(\Delta x, \Delta t)$ plot for $\Delta t = 7.5\tau_B$. Triangles represent simulated data; solid black lines represent four different fitted peaks. (b) $lnG(\Delta y, \Delta t)$ vs. Δy with $\Delta t = 0.1\tau_B$ (circles), $\Delta t = 2.0\tau_B$ (squares), $\Delta t = 7.5\tau_B$ (triangles) for $\beta V_0 = 1.0$. Inset: Linear fitting of $lnG(\Delta y, 7.5\tau_B)$ vs. Δy. Triangles represent simulated data and solid lines (black) represent two different fitted lines. (c) $lnG(\Delta x, \Delta t)$ vs. Δx with $\Delta t = 0.1\tau_B$ (circles), $\Delta t = 2.0\tau_B$ (squares), $\Delta t = 7.5\tau_B$ (triangles) for $\beta V_0 = 10.0$. (d) $lnG(\Delta y, \Delta t)$ vs. Δy with $\Delta t = 0.1\tau_B$ (circles), $\Delta t = 2.0\tau_B$ (squares), $\Delta t = 25.0\tau_B$ (triangles) for $\beta V_0 = 10.0$.

of the particles from trapping sites where the escape probability falls exponentially with potential strength. On the other hand, the diffusion in the transverse direction would be governed by local density of the particles at the potential minima. Since the particle accumulation would depend on potential strength via the Boltzmann factor, one would expect an exponential dependence of D_y on βV_0.

I examine the self-vHfs in presence of the external potential both in x- and y- directions as given by Eq. (6) to extract more complete dynamic information. I observe non-gaussian self-vHfs in different cases. I show $lnG_s(\Delta x, \Delta t)$ for three different reprensentative Δt's for $\beta V_0 = 1.0$ in Fig. 5(a) and $lnG_s(\Delta y, \Delta t)$ in Fig. 5(b).

I observe that for very small Δt (=$0.1\tau_B$, circles) $lnG_s(\Delta x, \Delta t)$ is parabolic in Δx, indicating a Gaussian $G_s(\Delta x, \Delta t)$.

At larger Δt ($= 2\tau_B$, squares), I observe that $lnG_s(\Delta x, \Delta t)$ has multiple peaks. More and more peaks appear at even larger Δt ($= 7.5\tau_B$, triangles). $lnG_s(\Delta x, \Delta t)$ data near the peaks fit to linear dependences in $(\Delta x)^2$ with different slopes as illustrated in inset of Fig. 5(a), suggesting multiple gaussian $G_s(\Delta x, \Delta t)$. These peaks indicate preferred locations of the particles as per the peridocity of the external modulation. $lnG_s(\Delta y, \Delta t)$ in Fig. 5(b) shows parabolic dependence below a critical value $< \Delta y_c = 0.7$ and linear dependence above this, suggesting an exponential tail in $G(\Delta y, \Delta t)$ for small Δt ($= 0.1\tau_B$, circles). Thus, there is a cross-over from gaussian self-vHf to that with an exponential tail. I find double linear dependence of $lnG_s(\Delta y, \Delta t)$ in Δy indicating a double exponential self-vHf at $\Delta t = 2.0\tau_B$, (squares, Fig. 5(b)). This double linear dependence is shown in inset of Fig. 5(b). Such behaviour persists even at $\Delta t = 7.5\tau_B$ (triangles, Fig. 5(b)).

$lnG_s(\Delta x, \Delta t)$ vs. Δx in Fig. 5(c) for $\beta V_0 = 10.0$ at smaller Δt ($= 0.1\tau_B$) shows double parabolic dependences (circles). These peaks get more prominent with increasing Δt(=$2\tau_B$, squares and =$7.5\tau_B$, triangles). Less number of peaks here indiactes slower motion of the particles for larger modulation so that the particles can not explore too many potential minima in the given time window. $lnG_s(\Delta y, \Delta t)$ in transverse direction for $\beta V_0 = 10.0$ in Fig. 5(d), show similar feature as in the lower modulation. I notice linear tail in Δy at smaller Δt ($= 0.1\tau_B$, circles). A double parabolic dependence is observed at $\Delta t = 2\tau_B$ (squares), persisisting at much larger Δt ($= 25.0\tau_B$, triangles).

Non-gaussian self-vHfs are interpreted as dynamic heterogeneity in a system[37]. In such systems there is coexistence of different regions where the diffusion coefficients are slightly different from each other. The heterogeneous particle motions are tracked from their displacements. I consider two particle configurations at time t and $t + \tau_B$. The probability distribution of magnitude of particle displacements between these two frames is constructed. Let $\langle \Delta r \rangle$ be the mean and σ' the standard deviation of the distribution. I identify those particles as fast whose displacements $|\Delta r| > \langle |\Delta r\rangle + \sigma'/2$ and those as slow whose displacements $|\Delta r| < \langle |\Delta r\rangle - \sigma'/2$. I show the fast and slow particles in Fig. 6 for large t. The fast and slow particles are shown by solid and open circles respectively. Fig. 6(a) is the configuration at $t = 20\tau_B$ for $\beta V_0 = 1.0$ and Fig. 6(b) the configurations at the same value of t for $\beta V_0 = 10.0$. I observe that in case of $\beta V_0 = 1.0$ both the fast and slow particles form small domains. In case of higher βV_0 (Fig. 6(b)) the domains are elongated parallel to y-direction. Thus, there are particles coexisting in the system with different mobilities.

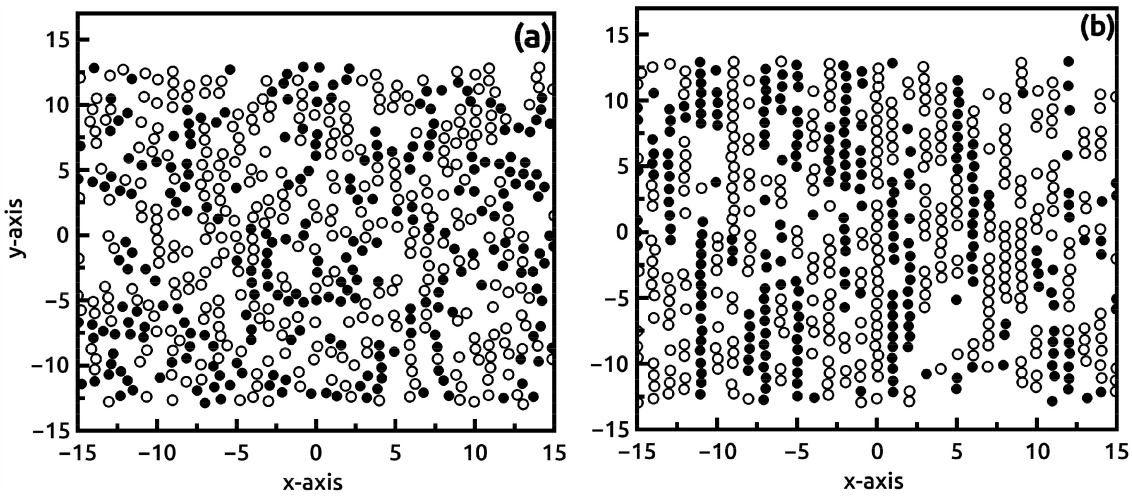

FIG. 6: Slow (open circle) and fast (solid circle) particles in equilibrium configuration of the system at $t = 20\tau_B$ for (a) $\beta V_0 = 1.0$ and (b) $\beta V_0 = 10.0$.

I examine the signature of dynamic heterogeneity in the system also from the residence times of the particles. The probability distributions of residence times along both parallel ($P(\tau_x)$) and transverse ($P(\tau_y)$) directions are shown in Fig. 7(a). Both $P(\tau_x)$ (dotted black line, Fig. 7(a)) and $P(\tau_y)$ (dotted dark grey line, Fig. 7(a)) have almost same peak height and identical mean value [$\langle\tau_x\rangle$ and $\langle\tau_y\rangle \simeq 3.70\tau_B$] in absence of external potential. This is similar to self-diffusion times $\tau_d = \frac{d^2}{2D_x} = \frac{d^2}{2D_y} = 4.5\tau_B$. Fig. 7(a) further shows $P(\tau_x)$ and $P(\tau_y)$ for $\beta V_0 = 1.0$. The peak height of $P(\tau_x)$ decreases along with a long tail extending upto about $30\tau_B$ (solid black line, Fig. 7(a)). $P(\tau_y)$ (solid dark gray line, Fig. 7(a)) shows similar nature, albeit with a faster fall. I observe different behaviour for $\beta V_0 = 10.0$. Here the dynamics is so slow that most of the particles take whole simulation time to diffuse the length of their diameter, suggesting the residence time for movement in x-direction diverges in the simulation time (data not shown). However, $P(\tau_y)$ vs. τ_y, shown in inset of Fig. 7(a), exhibits a peak around $\tau_y = 10\tau_B$ for this modulated strength with a much slower fall than the $\beta V_0 = 1.0$ case.

The variances of $P(\tau_x)$ and $P(\tau_y)$, denoted by $\sigma^2_{\tau_x}$ and $\sigma^2_{\tau_y}$, computed with respect to the peaks of $P(\tau_x)$ and $P(\tau_y)$, are shown in Fig. 7(b). The variances indicate dispersions in the residence times suggesting heterogeneity in particle motion. At lower βV_0, $\sigma^2_{\tau_x}$ is small due to homogeneous motion of the particles. In the intermediate βV_0, $\sigma^2_{\tau_x}$ is quite large with a broad peak around $\beta V_0 = 2.0$. This regime of βV_0 corresponds to the rise in ρ_{max} (Fig. 2(b)). Although the particles tend to populate the potential minima with increasing βV_0, a lot of particles stay away from the minima in this regime. The particles residing outside the trapping region have different mobilities than those located at the minima due to differences in the external potential at different locations. This leads to large variation of residence

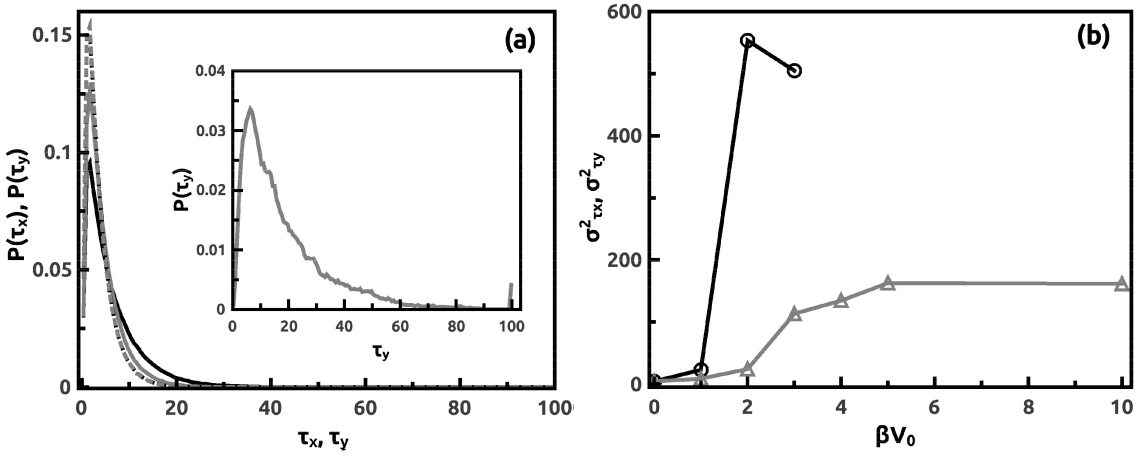

FIG. 7: (a) Probability distribution of residence times, $P(\tau_x)$ vs. τ_x (dotted black line) plot and $P(\tau_y)$ vs. τ_y (dotted dark grey line) for $\beta V_0 = 0.0$; $P(\tau_x)$ vs. τ_x (solid black line) plot and $P(\tau_y)$ vs. τ_y (solid dark grey line) for $\beta V_0 = 1.0$. Inset : $P(\tau_y)$ vs. τ_y plot. $\beta V_0 = 10.0$. (b) Variance, $\sigma^2_{\tau_x}$ vs. βV_0 (black line with black circles) and $\sigma^2_{\tau_y}$ vs. βV_0 (dark grey line with dark gray triangles) plot (with respect to mode of distribution).

times. At larger βV_0, the particles are strongly confined to the minima of the potential corresponding to saturation region in Fig. 2(b), homogenizing particle motions that leads to decrease in $\sigma^2_{\tau_x}$. This holds till the external potential is too strong to allow any particle motion where the residence time is comparable to the simulation time.

$\sigma^2_{\tau_y}$, on the other hand, as can be seen in Fig. 7 (b), increases with increasing βV_0 and then saturates beyond $\beta V_0 = 4.0$. The behaviour of $\sigma^2_{\tau_y}$ follows that of ρ_{max} in Fig. 2(b). The increase in the variance of the residence times with population of the particles indicates sluggish motion due to increasing particle numbers at the minima locations. The situation is akin to the case of glassy systems[45] and systems in the vicinity of jammimg transition[24, 25] where also the self-vHf show exponential tail for shorter time interval as observed in my system. The heterogeneity in transverse direction gets saturated beyond $\beta V_0 = 4.0$ where the particle density at the minima of the external potential gets saturated (Fig. 2(b)). Saturation of MSD along the modulation direction and single-file MSD in the transverse direction take over in this regime.

V. CONCLUSION AND OUTLOOK

In summary, I study, using BD simulations, dynamics of a two dimensional colloidal film periodically modulated in one direction. The density profiles ensure modulated liquid phase. The dynamics becomes slow in both the directions with increasing βV_0 and the diffusion coefficients decay exponentially. The self-vHf data show non-gaussian behaviour,

suggesting dynamical heterogeneity in the system. The dynamical heterogeneity is reflected in particles mobilities and residence times. Heterogeneous dynamics in modulation direction is due to pinning of the particles by the modulation potential, whereas that in the transverse direction is due to crowding the minima locations by the pinned particles. Such dynamical information can be of importance for the fabrication and development of microfluidic sensors[46–48], chips used in lab[49, 50] and sensing devices[51].

---

[1] A. Chowdhury, B. J. Ackerson and N. A. Clark, Phys. Rev. Lett. **55** 833 (1985).

[2] K. Loudiyi and B. J. Ackerson Physica A **184 1** (1992).

[3] J. Chakrabarti, H. R. Krishnamurthy and A. K. Sood, Phys. Rev. Lett. **73** 2923 (1994).

[4] J. Chakrabarti, H. R. Krishnamurthy, A. K. Sood and S. Sengupta, Phys. Rev. Lett. **75** 2232 (1995).

[5] C. Bechinger, M. Brunner and P. Leiderer, Phys. Rev. Lett. **86** 930 (2001).

[6] E. Frey, D. R. Nelson, and L. Radzihovsky, Phys. Rev. Lett. **83** 2977 (1999).

[7] L. Radzihovsky, E. Frey and D. R. Nelson, Phys. Rev. E **63** 031503 (2001).

[8] M. Schmiedeberg, J. Roth and H. Stark, Phys. Rev. Lett. **97** 158304 (2006).

[9] S. Deutschländer, T. Horn, H. Löwen, G. Maret and P. Keim, Phys. Rev. Lett. **111** 098301 (2013).

[10] C. B. Chaudhuri, S. Chakrabarty and J. Chakrabarti, J. Chem. Phys. **139** 204903 (2013).

[11] M. C. Jenkins and S. U. Egelhaaf, J. Phys.: Condens. Matter **20** 404220 (2008).

[12] R. F. Capellmann, A. Khisameeva, F. Platten and Egelhaaf 2018 J. Chem. Phys. **148** 114903 (2018).

[13] C. Bechinger and E. Frey J. Phys.: Condens. Matter **13** R321 (2001).

[14] H. Löwen J. Phys.: Condens. Matter **13** R415 (2001).

[15] H. Löwen Eur. Phys. J. ST **222** 2727 (2013).

[16] S. Herrera-Velarde and R Castañeda-Priego, Phys. Rev. E **79**, 041407 (2009).

[17] J. P. Hansen, I. R. McDonalds *Theory of simple liquids* (UK, Elsevier Academic Press) (1986).

[18] D. A. Stariolo and G. Fabricius, J. Chem. Phys. **125** 064505 (2006).

[19] J. D. Eaves and D. R. Reichman Proc. Natl Acad. Sci. USA **106** 15171 (2011)

[20] W. K. Kegel and A. van Blaaderen, Science **287** 290 (2000).

[21] E. J. Saltzman and K. S. Schweizer, Phys. Rev. E **77** 051504 (2008)

[22] E. R. Weeks, *et. al.* Science **287** 627 (2000).

[23] H. E. Castillo and A. Parsaeian, Nature Phys. **3** 26 (2007).

[24] P. Chaudhuri, L. Berthier and W. Kob, Phys. Rev. Lett. **99** 060604 (2007).

[25] D. J. Bray, M. R. Swift and P. J. King, Phys. Rev. E **75** 062301 (2007).

[26] Y. Yu, S. M. Anthony, S. C. Bae and S. Granick, J. Phys. Chem. B **115** 2748 (2011).

[27] P. I. Hurtado, L. Berthier and W. Kob, Phys. Rev. Lett. **98** 135503 (2007).

[28] Y. Gao and M. L. Kilfoil, Phys. Rev. Lett. **99** 078301 (2007).

[29] W. Chen and K. To, Phys. Rev. E **80** 061305 (2009).

[30] J. S. Van Zon and F. C. MacKintosh, Phys. Rev. Lett. **93** 038001 (2004).

[31] B. Liu and J. Goree, Phys. Rev. Lett. **100** 055003 (2008).

[32] F. Rouyer and N. Menon, Phys. Rev. Lett. **85**, 3676 (2000).

[33] S. Dutta, J. Chem Phys. **522** 256-259 (2019).

[34] S. Dutta and J. Chakrabarti, Phys. Chem. Chem. Phys. **22** 17731-17737 (2020).

[35] S. Dutta and J. Chakrabarti, EPL **116** 38001 (2016).

[36] S. Dutta and J. Chakrabarti, Soft Matter **14** 4477-4482 (2018).

[37] B. Wang, J. Kuo, S. C. Bae and S. Granick, Nature Materials **11** 481 (2012).

[38] Dalle-Ferrier Cécile *et. al.*, Soft Matter **7** 2064

[39] F. Evers *et. al.* Eur. Phys. J. Special Topics **222** 2995 (2013).

[40] B. V. Derjaguin, N. V. Churaev and V. M. Muller *The DerjaguinLandauVerweyOverbeek (DLVO) Theory of Stability of Lyophobic Colloids* In: Surface Forces. Springer, Boston, MA, (1987).

[41] C. Das, P. Chaudhuri, A. K. Sood, and H. R. Krishnamurthy, Curr. Sci. **80** 959 (2001).

[42] Q. H. Wei, C. Bechinger and P. Leiderer, Science **287** 625 (2000).

[43] C. Lutz, M. Kollmann and C. Bechinger, Phys. Rev. Lett. **93** 026001 (2004).

[44] C. Mondal and S. Sengupta, Phys. Rev. E **85** 020402(R) (2012).

[45] B. Wang, S. M. Anthony, S. C. Bae and S. Granick, Proc. Natl Acad. Sci. USA **106** 15160 (2009).

[46] A. Terray, J. Oakey, and D W M Marr, Science **296** 1841 (2002).

[47] A. Terray, J. Oakey, and D W M Marr *Appl. Phys. Lett.* **81** 1555 (2002)

[48] S. Chen, Z. Wang Z, X. Cui *et al.* Nanoscale Res. Lett. **14** 71 (2019).

[49] S. K. Lee, G. R. Yib and S. M. Yang, Lab Chip **6** 1171 (2006).

[50] S. K. Hoi, X. Chen, *et. al.* Adv. Funct. Mater. **21** 2847 (2011).

[51] M. Grzelczak and Liz-Marzán Luis M Langmuir **29** 4652 (2013).

Chapter 4: Remixing of a phase separated binary colloids in an external modulation*

I. INTRODUCTION

In the previous chapter I report on a mono-disperse colloidal suspension under external modulation. Here I explore phase and dynamic nehaviour of a binary colloidal system under external modulation. However, the miscibility in colloidal mixtures in presence of external perturbations has not been considered so far.

Numerous demixing studies have been reported on colloidal mixtures. There have been studies on demixing of model colloids composed of two different sizes of polystyrene spheres using diffusing wave spectroscopy [1]. Experiments have been done on a binary dispersion of like-charged colloidal particles under very low salt condition. The particles have similar size but large charge asymmetry. They have been found to exhibit phase separation into crystal and fluid phases. Here the colloid-ion interactions provide a driving force for crystallization of one species[2]. Confocal microscopy studies on demixing and remixing with temperature in binary liquids containing colloidal particles has been reported [3, 4].

Experiments have been reported on binary systems with colloidal particles of different sizes subject to a spatially periodic potential, using the external modulation generated in a given direction by interfering laser beams[5]. The wavelength of the modulation is equal to the size of the bigger particles, and the modulation is stronger for them than the smaller particles. It is observed that an increase in the external modulation amplitude leads to localization of the large particles analogous to a modulated liquid with an increasing fraction of small particles caged by the bigger particles. The smaller particles arrange themselves in a triangular fashion inside those cages. The large particles are observed to remains ordered, whereas the lattice of small particles became disordered upon increasing the temperature. The dynamical studies on colloids are reported on non-equilibrium situations as in supercooled liquids[6], glassy systems[7, 8], sheared binary mixture at oil-water interface[9], lane forming binary colloids in electric field[10–12]. Many of these systems show dynamic heterogeneity where regions with not too different temporal relaxation rates co-exist in the system. Segregation and mixing in granular media has beed reported earler as well[13].

---

* S Pal, J Chakrabarti, arXiv preprint arXiv:2307.15450 (2023)

The mixing of the components in a binary colloidal system including both the structural and dynamical aspects, remain unexplored to the best of my knowledge.

In this backdrop I study a model binary system with different particles of diameter ratio 2:1 in an external modulation as in Ref.[5]. The external modulation wavelength is equal to the diameter of the big particles and the strength of modulation is twice for the big particles than the small ones. The interactions among the colloidal particles are short ranged repulsive potentials where the cross-species interactions are stronger than the intra-species interactions. I perform Monte Carlo (MC) (see section IB in chapter 2) simulations at room temperature to study the phase separation where the Metropolis sampling has been done based on the energy cost of a particle movement due to interaction with all other particles and the external modulation. I calculate pair correlation function, cluster size distribution and bond angle parameter to characterize structural changes in the system. I also compute thermodynamic quantities such as demixing order parameter and specific heat in order to investigate the phase transition when structural changes occur in the system. I further perform Brownian Dynamics (BD) simulations from the equilibrated MC structures and analyse the dynamics of different species of particles by means of mean square displacement (MSD) as the system evolves in time.

The components are observed to demix in absence of any external modulation potential. The bigger particles align themselves along the potential minima, while the clusters of the smaller particles break into smaller clusters in presence of external potential. There is triangular arrangement among the small particles within the clusters. The mean cluster size of the smaller particles and the demixing order parameter shift to lower values, suggesting remixing of the species with increasing field strengths. The demixing order parameter shows a discontinuity and the specific heat shows a peak that grows as the system size increases, suggesting the presence of a thermodynamic first order phase transition with increasing modulation strength. The dynamics, however, is observed to be diffusive for both the type of particles which decrease with increase in strength of modulation.

The chapter is organised as follows: I introduce the system and provide its details in section II. I discuss the structural properties like configuration, isotropic and anisotropic pair correlation function, cluster size analysis and the thermodynamic quantities like demixing order parameter and specific heat in section III followed by the dynamic properties in section IV. Sec V concludes the chapter.

II. SYSTEM DETAILS

The particles interact via repulsive potential of the form:

$$V^{(\alpha\beta)}(r_{ij}) = 4\epsilon_{\alpha\beta}(\frac{\sigma_{\alpha\beta}}{r_{ij}})^{12} \tag{1}$$

Here r_{ij} is the distance between i^{th} and j^{th} particles belonging to species α ($= b$ for big particles and s for the small particles) and $\beta(= b, s)$ respectively, $\epsilon_{\alpha\beta}$ the strength of the mutual repulsive interaction and $\sigma_{\alpha\beta}$ the diameter of the particles used in simulation. Here $\alpha = \beta$ corresponds to the particles of the intra-species, while $\alpha \neq \beta$ corresponds to the cross species interactions. I take $\sigma_{bb} = D_b, \sigma_{ss} = D_s$ and $\sigma_{bs} = 0.5(\sigma_{bb} + \sigma_{ss})$, D_b and D_s being the diameter of the big and small particles respectively. I further subject the system to an external spatially periodic potential of the form:

$$V^{\alpha}_{ext}(x) = -V^{\alpha}_0 cos(\frac{2\pi x}{\lambda}), \tag{2}$$

where x denote the x-coordinate of the particles, λ the wavelength of the external potential equal to the diameter of the bigger particles and V^{α}_0 the amplitude of the external potential on α^{th} particle. I take $V^b_0 = V_0 = 2V^s_0$ as in Ref.[5]. I take $D_b(= 5\mu m)$ and $D_s(= 2.5\mu m)$[5]. The packing fraction, $\phi[= (N_b/4\pi D_b^2 + N_s/4\pi D_s^2)/A$, where A is the area of the system] $= 0.72$[5]. I take equal number of big and small particles, $\frac{N_b}{N_s} = 1.0$[5].

D_s is taken as the unit of length and K_BT at room temperature (T=300K) as the unit of energy. I fix $\frac{\epsilon_{bb}}{K_BT} = \frac{\epsilon_{ss}}{K_BT} = 1.0$ and vary $\frac{\epsilon_{bs}}{K_BT}$ in the range of 0.5 to 1.5, the exact values being mentioned as appropriate.. Most of the results are reported on N=1024 particles. Monte Carlo (MC) simulations are carried to study the phase behaviour of a system of particles with equal number of big and small particles ($N_b = N_s$) in a box of reduced length in x-direction, $\frac{L_x}{D_s}(= 58.0)$ that comprises of 29 wavelengths for 1024 number of particles and that in y-direction $L_y = \frac{\sqrt{3}}{2}L_x$. I take the cut-off value for the interaction to be $r_c = 5\sigma_{ss}$. I run for a total of 10^6 MC steps where the equilibration is judged from the energy values. Different quantities of interests are calculated over the 200000 equilibrated configurations and averaged over five independent runs. I also study the system for N=144 with 11 wavelengths and N=4096 with 58 wavelengths keeping the area fraction fixed to check system size dependencies of different quantities.

I further carry out Brownian Dynamics (BD) (see section IB in chapter 2) simulation for the system using the

discretized Langevin equation in the over-damped equation of motion for the ith particle of particle of species α as:

$$\gamma_\alpha \dot{\vec{r}}_{i\alpha} = \vec{F}_i^{\alpha^{int}} + \vec{F}_i^{\alpha^{rand}} + \vec{F}_i^{\alpha^{ext}} \tag{3}$$

where $\vec{F}_i^{\alpha^{int}} = -\vec{\nabla}_i^\alpha \Sigma_{ij} V(r_{ij})$ is the force due to systematic interaction among the colloidal particles, Δt the time interval for integration, and $\gamma_\alpha (= 6\pi\eta D_\alpha)$ are the damping factors with the viscosity coefficient $\eta = 1$ CP corresponding to water., $\vec{F}_i^{\alpha^{rand}}$ is the force on the two types of particles due to random bombardment of solvent particles on them and $\vec{F}_i^{\alpha^{ext}}$ is the force due to the external modulation. I take τ_s, the diffusion time of the smaller particles as reduced unit of time. I run for a total of 10^7 BD steps taking integration time step $\Delta t = 0.0001$ in reduced unit. The equilibration is judged from the energy values. I calculate the mean squared displacements (MSD) of the particles along both x and y-directions from their displacements in starting from an initial time t_0 :

$$\langle (\Delta x_\alpha)^2 \rangle = \langle \frac{1}{N_\alpha} \Sigma_i (x_i^\alpha(t) - x_i^\alpha(t_0))^2 \rangle \tag{4}$$

and

$$\langle (\Delta y_\alpha)^2 \rangle = \langle \frac{1}{N_\alpha} \Sigma_i (y_i^\alpha(t) - y_i^\alpha(t_0))^2 \rangle. \tag{5}$$

The average is taken over the 15 initial times t_0 chosen 10^4 steps apart for a given trajectory and five independent Brownian trajectories.

III. STRUCTURAL PROPERTIES

I check the equilibrium in MC simulation from energy data for different βV_0 for N=1024 particles. Let us consider the system in absence of external potential ($\beta V_0 = 0.0$). Although the potentials are additive, they are taken to be non-ideal, the cross-species interactions being different from the intre-species interactions, not following the Lorentz-Berthelot rule. Fig. 1(a) shows a typical particle arrangement in equilibrium for $\epsilon_{bs} = 1.5$. The cross species interaction is stronger than intra-species interaction. I observe large clusters of small particles in the background of the big particles. I do not observe complete demixing due to strong intra-species repulsion. Next I consider the case $\epsilon_{bs} = 0.5$, where the cross-species interaction is weaker than the intra-species interaction. Fig. 1(b) shows

an equilibrium configuration in such conditions. I observe a mixture of bigger and smaller particle. Thus, the non-ideality in interaction with stronger cross-species interaction leads to the demixing in the case, similar for non-additive interaction[14**?**].

Let us now consider the effect of the external potential starting from the configuration with $\epsilon_{bs} = 1.5$ where the smaller particles form large clusters. I show equilibrated snapshot for $\beta V_0 = 4.0$ in Fig. 1(c).

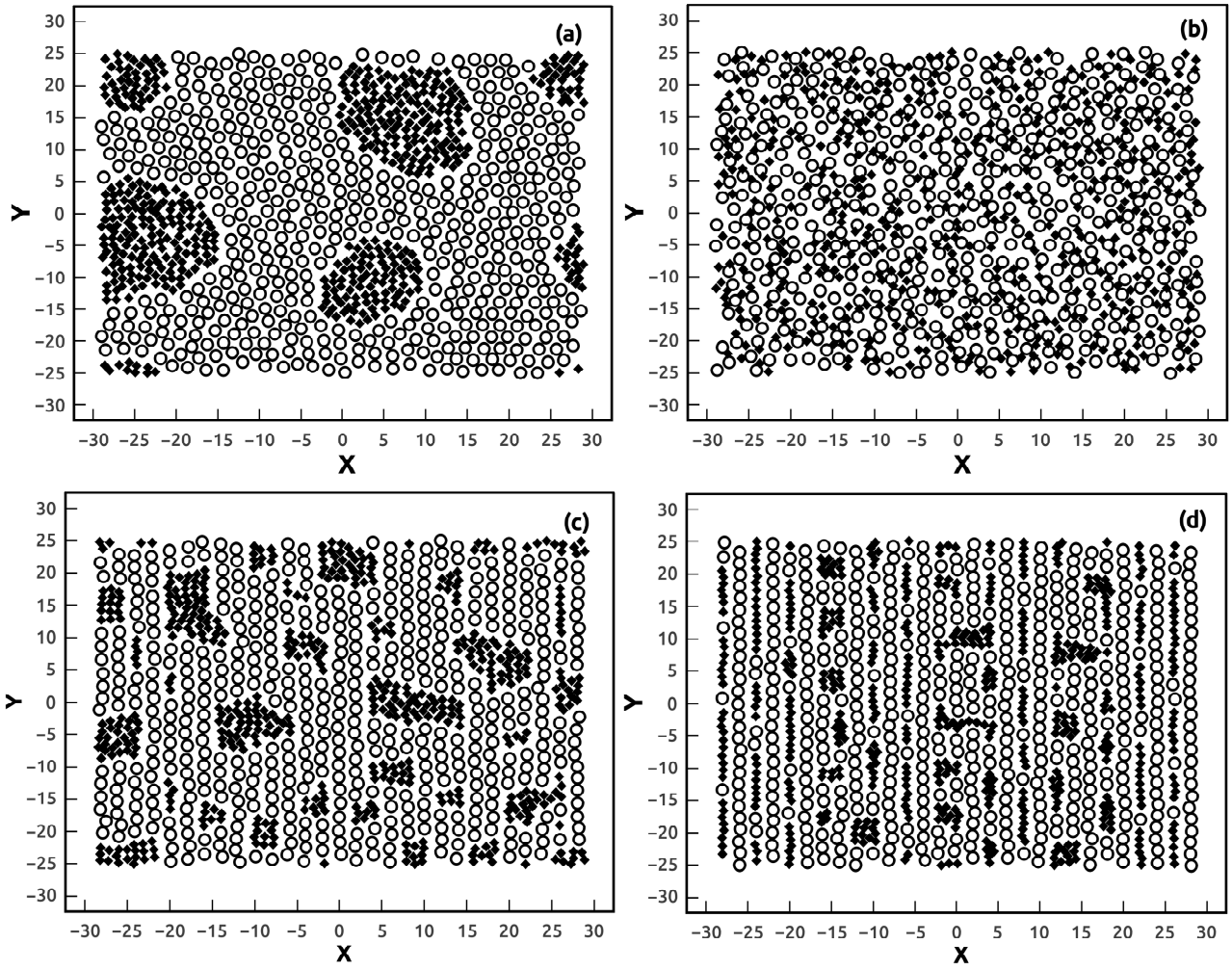

FIG. 1: Final configuration with $\epsilon_{bs} = 0.5$ at (a) $\beta V_0 = 0.0$, with $\epsilon_{bs} = 1.5$ at (b) $\beta V_0 = 0.0$, (c) $\beta V_0 = 4.0$, (d) $\beta V_0 = 10.0$ with bigger (open circle) and smaller particles (close rhombi).

The snapshot shows that the big particles are aligned along the potential minima due to the matching of wavelength of external potential to the big diameter and stronger modulation strength than the smaller particles. The big clusters

of the smaller particles break into smaller clusters to make way for the bigger particles. This tendency of mixing is further enhanced as I increase the strength of the potential further to $\beta V_0 = 10.0$ as shown in Fig. 1(d). It may be noted that the particles arrange without any spatial order along y direction suggesting modulated fluid phases similar to those reported earlier[15, 16]. I also look into density contour plots for both the species in Fig. 2 (a)-(b). I observe patches of big clusters of smaller particles in the background of bigger ones for $\beta V_0 = 0.0$ (Fig. 2(a)). With stronger modulation ($\beta V_0 = 10.0$), the modulated mixed phase is observed from Fig. 2(b) with both bigger and smaller particles around the external potential minima without any seggregation.

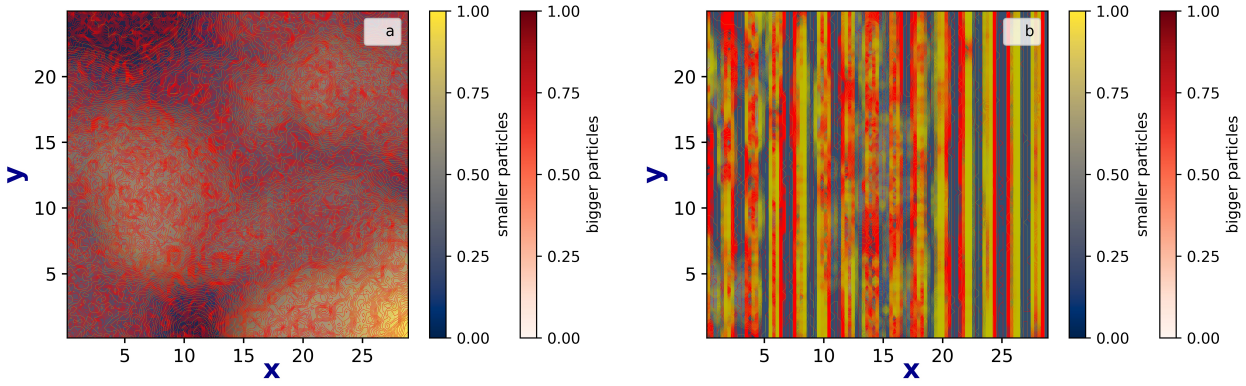

FIG. 2: Density contour plot for N=1024 at (a) $\beta V_0 = 0.0$ and (b) $\beta V_0 = 10.0$.

Pair correlation function

I characterise the structural correlations from the histograms of the separation between particle pairs, also called the radial distribution function (rdf) $g_{\alpha\beta}(r)$ [17]. This quantity describes the probability of finding a pair of particles belonging to species α and β at separation r. Fig. 3(a)-(c) shows isotropic rdf for big-big $g_{bb}(r)$, small-small $g_{ss}(r)$, big-small $g_{bs}(r)$ pair of particles in absence of external potential. I observe liquid-like short ranged structural behaviour in both $g_{bb}(r)$ and $g_{ss}(r)$. However, $g_{bs}(r)$ is much weaker. This means that the two species do not find themselves in the vicinity of each other due to phase separation between them.

The system becomes anisotropic in presence of the external modulation. The anisotropic structure of the system is characterized by the pair correlation functions (PCF) in Figs. 3(d)-(f). They are obtained by binning the pair separations both in x- and y-directions. It may be noted that the rdf is the circular symmetric counter-part of the PCF. $g_{bb}(x, y)$ (Fig.3(d)) shows parallel strips along potential minima as per the periodicity of the external potential.

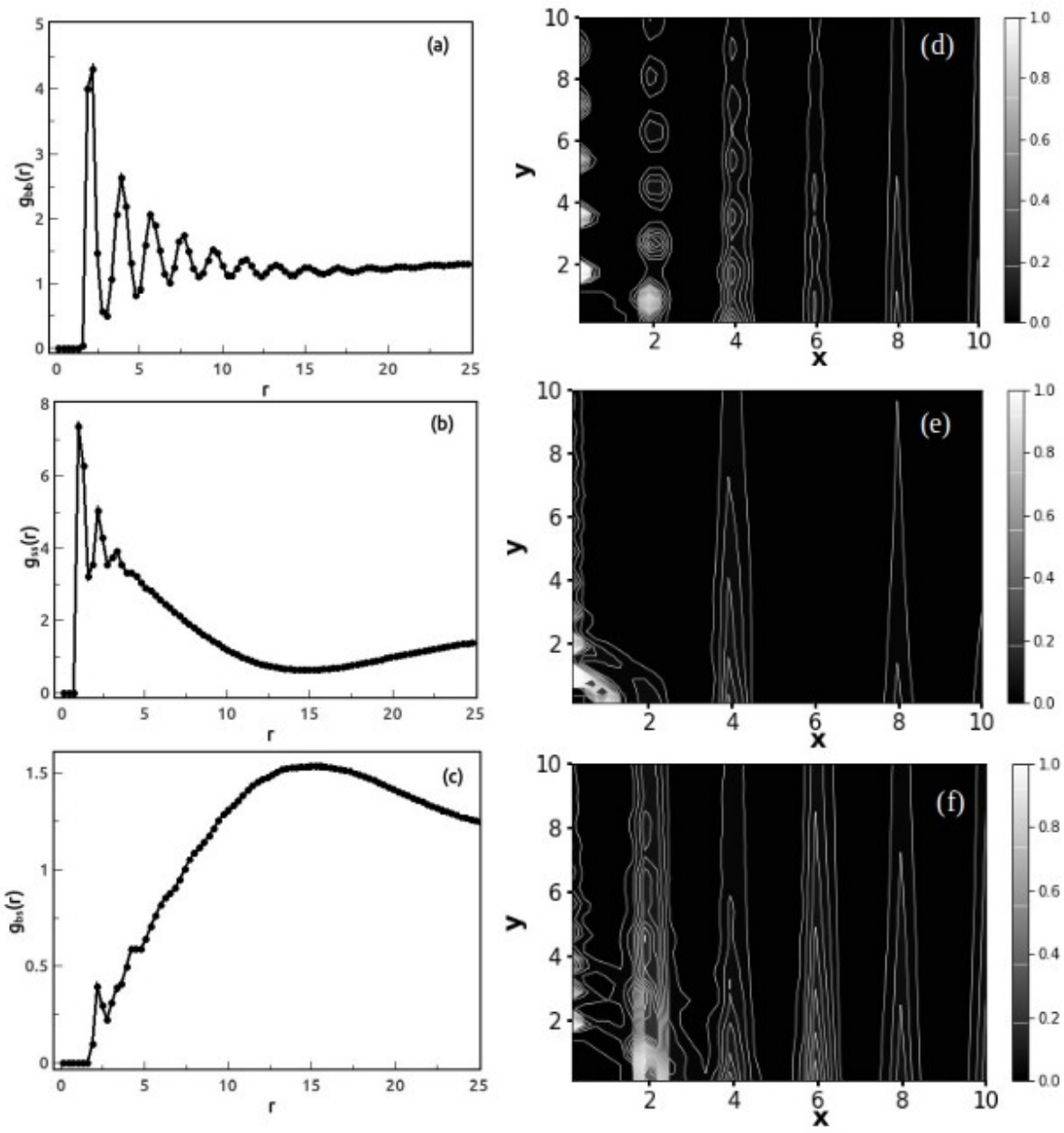

FIG. 3: Isotropic RDF for $\beta V_0 = 0.0$: (a) $g_{bb}(r)$ (big-big), (b) $g_{ss}(r)$ (small-small) and (c) $g_{bs}(r)$ (big-small interaction); and anisotroopic PCF for $\beta V_0 = 10.0$: (d) $g_{bb}(x, y)$ (big-big) , (e) $g_{ss}(x, y)$ (small-small) and (f) $g_{bs}(x, y)$ (big-small interaction).

$g_{ss}(x, y)$ in Fig. 3(e) shows dark patches on overall circular pattern, signifying deviation from isotropic structure. Due to breaking of clusters, the smaller particles arrange themselves nearer the bigger species as shown in Fig 1(c) and 1(d). This leads to strong big-small correlations $g_{bs}(x, y)$ (Fig. 3(f)).

The alignment tendency of the particles is quantified by the relative orientation (θ_{ij}) between i^{th} and j^{th} particles

with respect to modulation direction, $\theta_{ij} = tan^{-1}(\frac{y_j - y_i}{x_j - x_i})$. I plot distribution $P^{(\alpha)}(\theta)$ of bond angle θ considering θ_{ij} for all the pairs of the α_{th} species over equilibrium configurations. I show $P^{(b)}(\theta)$ vs. θ for bigger particles in the main panel of Fig. 4 and $P^{(s)}(\theta)$ vs. θ for smaller particles in inset of the same figure for $\beta V_0 = 0.0$. Both $P^{(b)}(\theta)$ and $P^{(s)}(\theta)$ at $\beta V_0 = 0.0$ are flat with no distinct peak. I show in Fig. 5(a) and (b) the distribution $P^{(\alpha)}(\theta)$.

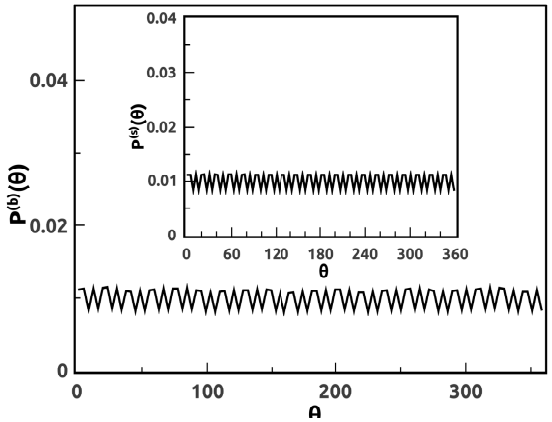

FIG. 4: Big-big bond angle distribution $P^{(b)}(\theta)$ for $\beta V_0 = 0.0$; inset : small-small bond angle distribution $P^{(s)}(\theta)$ for $\beta V_0 = 0.0$.

Fig. 5(a) shows data for the big particles $P^{(b)}(\theta)$ in the main panel and for small particles $P^{(s)}(\theta)$ in inset for both $\beta V_0 = 5.0$. The strong peaks in $P^{(b)}(\theta)$ at $\theta = 90°$ and $\theta = 270°$ are equivalent to one another, reflecting like mirror images about $\theta = 180°$. This indicates alignment of bigger particles along the minima of the external potential. $P^{(s)}(\theta)$ versus θ for smaller particle (inset of Fig. 5(a)) shows strong peaks at $\theta = 90°$ and $\theta = 270°$ and smaller peaks at $\theta = 30°$ and $\theta = 150°$, symmetric about $\theta = 180°$. This suggests that the smaller particles form clusters with a local triangular arrangement among themselves, similar to observations reported in earlier experimental work [5]. Similarly Fig. 5(b) shows data for the big particles $P^{(b)}(\theta)$ in the main panel and for small particles $P^{(s)}(\theta)$ in inset for both $\beta V_0 = 10.0$. The alignment tendency increases leading to stronger peak in both $P^{(b)}(\theta)$ and $P^{(s)}(\theta)$ at $\theta = 90°$ and $\theta = 270°$ for bigger and smaller particles respectively at $\beta V_0 = 10.0$.

Mixing behaviour

Next I characterize the breaking of the small particle clusters. I compute the size of clusters C of the small particles as follows. I take the small particles to belong to a cluster whose centre to centre distances in x- and y-direction are less than x_{cl} and y_{cl} respectively. I choose $x_{cl} = 1.25$. Here x_{cl} corresponds to the first minimum in $g_{ss}(x, y)$ and $y_{cl} = \frac{\sqrt{3}}{2} x_{cl}$ considering the anisotropy in the system. I show distribution $P(C)$ for smaller particles in Fig. 5(c)

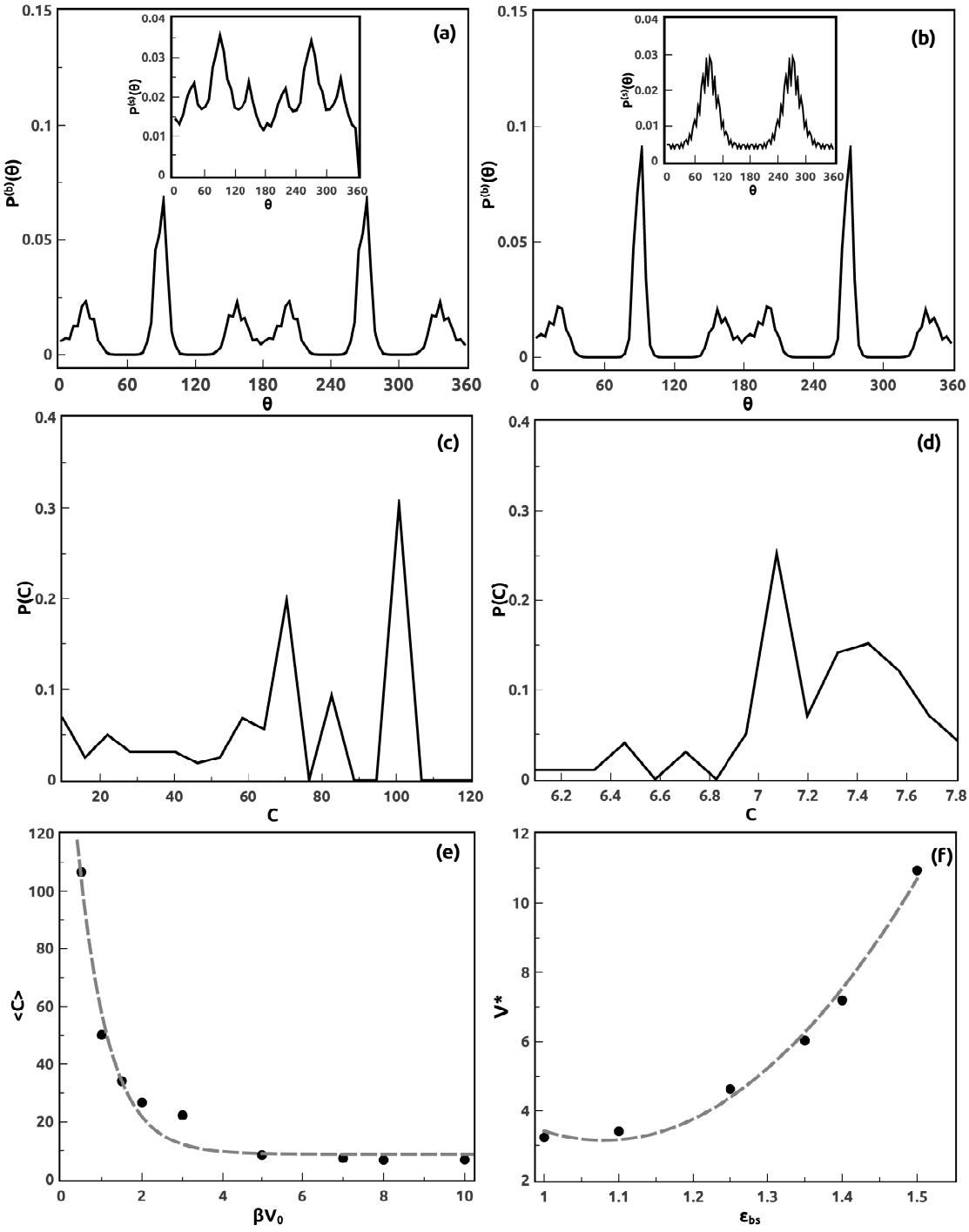

FIG. 5: (a) Big-big bond angle distribution $P^{(b)}(\theta)$ for $\beta V_0 = 5.0$; inset : small-small bond angle distribution $P^{(s)}(\theta)$ for $\beta V_0 = 5.0$, (b) Big-big bond angle distribution $P^{(b)}(\theta)$ for $\beta V_0 = 10.0$; inset : small-small bond angle distribution $P^{(s)}(\theta)$ for $\beta V_0 = 10.0$. Cluster size distribution of smaller particles $P(C)$ at (c) $\beta V_0 = 0.0$, (d) $\beta V_0 = 10.0$, (e) Average cluster size $< C >$ vs. βV_0 with exponential decay as fitted as $< C >= 121.51 e^{-0.81(\beta V_0)}$ (f) V^* vs. ϵ_{bs} with power law dependence as $V^* \sim \epsilon_{bs}^{2.38}$ where V^* is the simulated critical strength of modulation where the average cluster size falls to $\frac{1}{e}^{th}$ of the maximum value.

and 5(d) for two different βV_0(=0.0 and 10.0 respectively). Large clusters of the smaller particles are observed in Fig 5(c) in agreement to phase separation between two species in absence of external modulating potential. It is clear that the distribution peaks are shifted to lower values of cluster sizes C for βV_0(= 10.0)(inset Fig. 5(d)). I plot the mean cluster size $\langle C\rangle (= \int CP(C)dC)$ versus βV_0 in Fig. 5(e). I observe that $\langle C\rangle = Ae^{-B(\beta V_0)}$ with $A = 121.51$ and $B = 0.81$. Note that $< C >$ falls to $\frac{1}{e}$ at $V^* = \beta V_0 = 1/B$ as shown in Fig. 5(e).

I repeat my simulation for other ϵ_{bs} values keeping the intra-species interaction fixed. I plot V^* for different ϵ_{bs} in Fig. 5(f). I observe that $V^* \sim \epsilon_{bs}^{2.4}$ as can be seen in the fitted curve in Fig. 5(f). Physically, the big particles tend to get aligned more strongly than the small ones, making their ways splitting through the clusters of smaller particles with increasing βV_0. The surface energy cost of this breaking up is supported by the external potential. Let us consider for simplicity the case that a cluster of radius R breaks into two of radii r_1 and r_2. The change in line energy is given by:$\Delta f = 2\pi\Sigma(r_1 + r_2 - R)$ where Σ is the coefficient of line tension. If I assume that the mean density ρ of the particles do not change due to breaking cluster and no particle is lost during the break up, then $r_1^2 + r_2^2 = R^2$. The minimum of the change in line free energy can be estimated by minimizing with respect to r_1. I find $\Delta f_{min} = 2\pi\Sigma R(\sqrt{2} - 1)$. The radius R of the droplet consisting of small particles in the background of the large particles can be stabilized if the total free energy, consisting of the droplet and the line tension components, is at minimum. If δg is the free energy per unit area of the droplet, then the bulk component $\sim \delta g R^2$. The line component $\sim \Sigma R$. The minimum of the free energy is achieved by $R = \Sigma/\delta g$. Hence, $\Delta f_{min} \sim \Sigma^2$. The line tension experienced by the droplet of the smaller particles in the background of the larger particles is proportional to ϵ_{bs} and consequently, $\Delta f_{min} \sim \epsilon_{bs}^2$. This amount of energy for breaking the droplet needs to be supplied through the external potential, implying that $\beta V_0 \sim \epsilon_{bs}^2$. This is consistent with the simulation observation.

I calculate the demixing order parameter for different βV_0. I partition the simulation box into small rectangular cells with dimension $\Delta x = 1.25$ and $\Delta y = \frac{\sqrt{3}}{2}\Delta x$. Let n_{ib} and n_{is} be the numbers of big and small particles in each of the boxes respectively. The demixing order parameter is defined as:

$$O_d = \frac{1}{N} < \Sigma_{i=1}^{M} |(n_{ib} - n_{is})| > . \tag{6}$$

Here N is the total number of particles, M the total number of partitions of the system and the averages are done on equilibrium configurations.

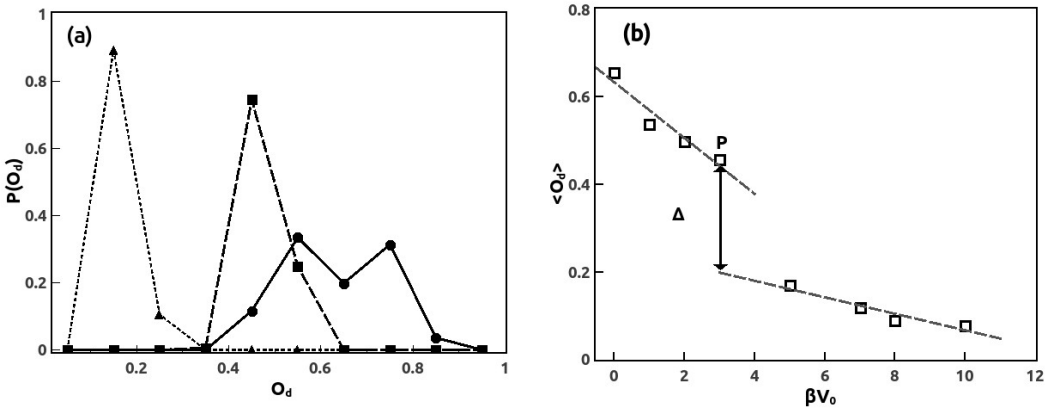

FIG. 6: (a) Distribution of demixing order parameter $P(O_d)$ at $\beta V_0 = 0.0$ (black solid line, solid circle), $\beta V_0 = 5.0$(black dashed line, solid square), $\beta V_0 = 10.0$(grey dotted line, solid triangle). (b) Average order parameter $< O_d >$ vs. βV_0 for N=1024

Fig. 6(a) shows the distribution $P(O_d)$ for all three cases of different βV_0. I observe a prominent peak at large O_d value for $\beta V_0 = 0.0$. The peak shifts to a lower O_d value, indicating mixing enhanced with βV_0. Fig. 6(b) shows the order parameter averaged over the configurations $\langle O_d \rangle$ vs βV_0. I observe that $\langle O_d \rangle$ decreases with βV_0 following two distinct branches, corresponding to low values and that to higher values with discontinuity around βV_0=4.0. This value is less than V* for the case of $\epsilon_{bs} = 1.5$ as can been seen from Fig. 5(f). Thus, phase transition occurs before the clusters are broken into very smaller ones corresponding to their sizes being $\frac{1}{e}^{th}$ of the maximum cluster size. The amount of discontinuity Δ in $\langle O_d \rangle$ is estimated as follows. I take the last simulated data point P of the upper branch and extrapolate the fitted curves of the lower branch to P. Then I take their difference in $\langle O_d \rangle$ at the simulated point and extrapolated point as Δ. This estimation is schematically drawn in Fig. 6(b).

I further simulate the system behaviour for different system sizes N=144 and N=4096. I also show snapshots for $\beta V_0 = 0.0$ for these two system sizes in Fig. 7(a) and (b). I observe that in absence of any external modulation, big clusters of smaller particles are forming in a background of bigger ones for both N. Those clusters are broken into smaller ones and as a result both the species mix together in presence of finite modulation strength as can be seen in Fig. 7 (c) and (d) at $\beta V_0 = 10.0$ for both N. Here, too, I observe similar phenomena of the system going from a phase separated one to a mixed one with βV_0.

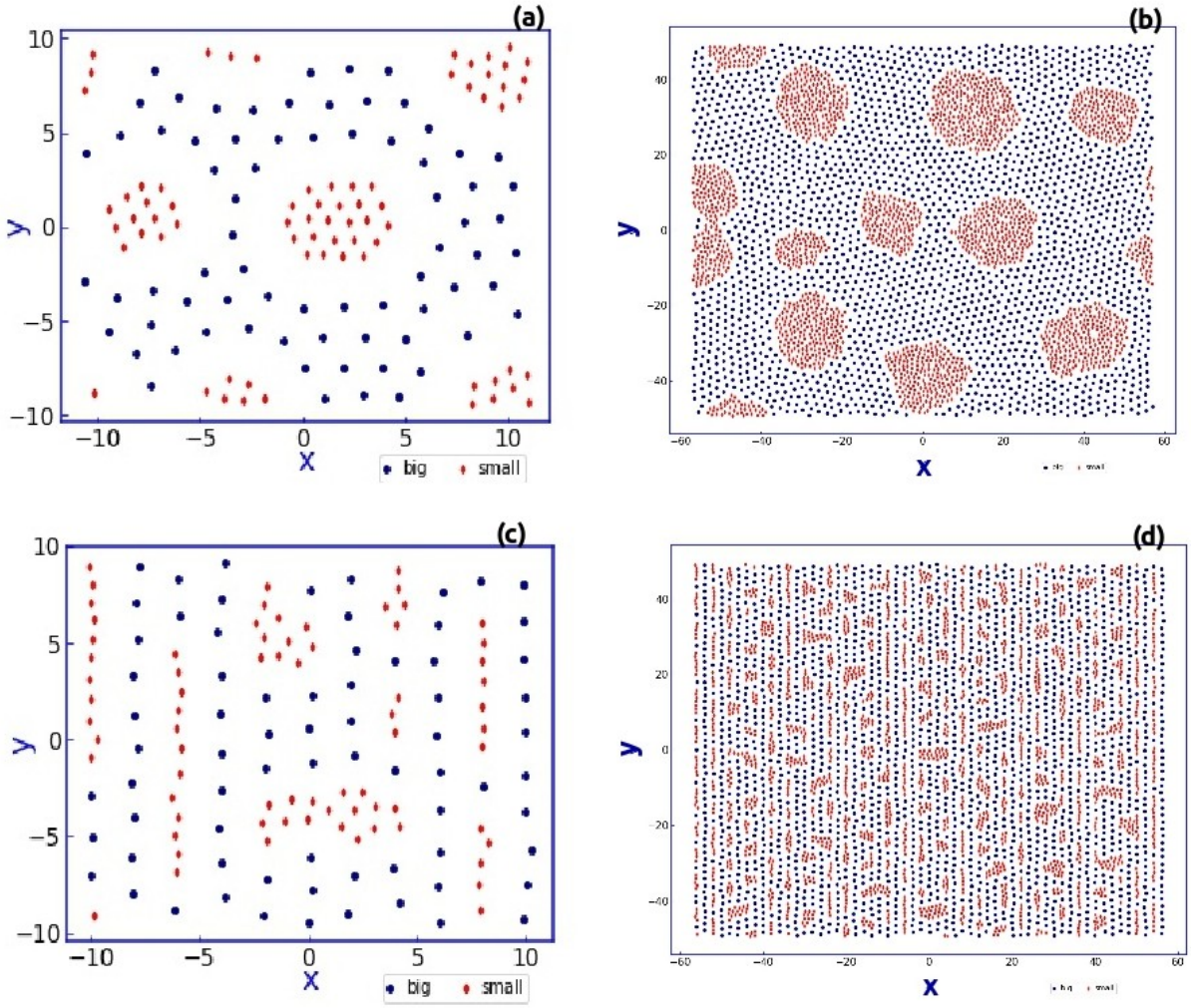

FIG. 7: Equilibrium MC configuratin at $\beta V_0 = 0.0$ for (a) N=144, (b) N=4096 and at $\beta V_0 = 10.0$ for (c) $\beta V_0 = 0.0$, (d) $\beta V_0 = 10.0$.

I also plot $g_{\alpha\beta}(r)$ for both the system sizes in the absence of external potential in Fig. 8(a)-(f) which show similar behaviour as those for N=1024.

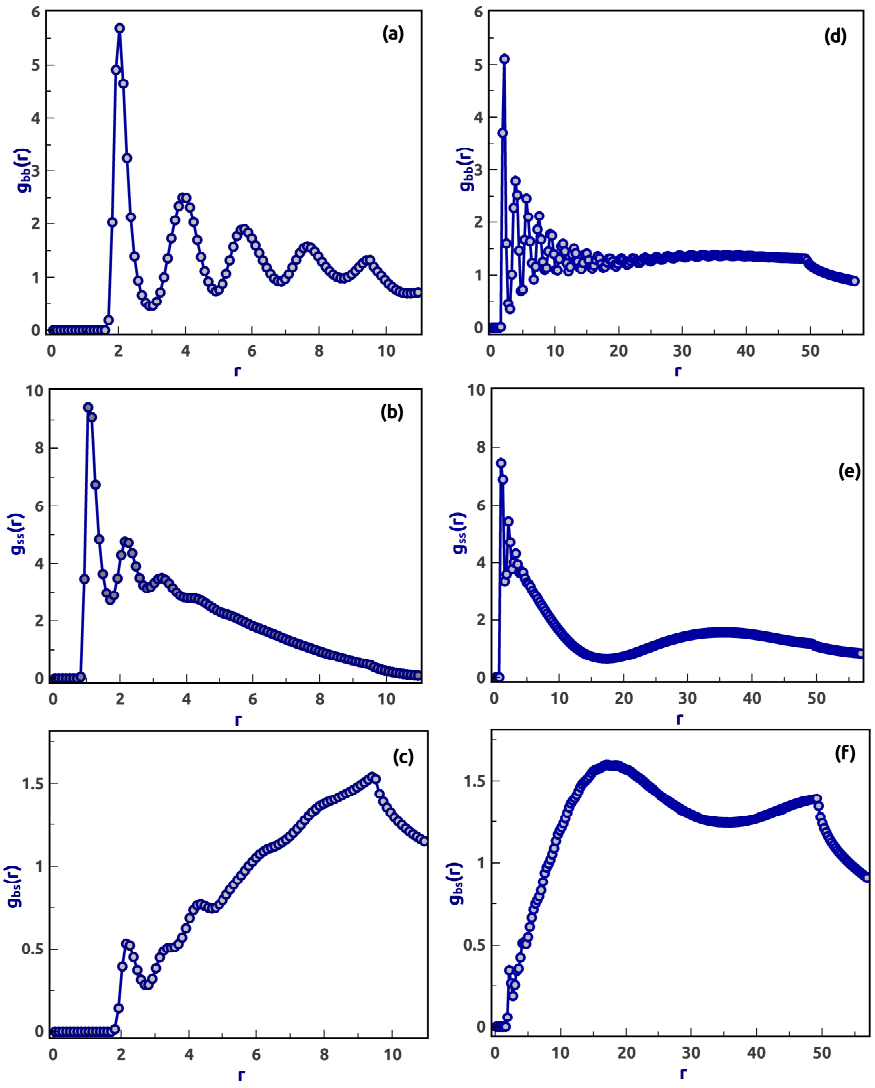

FIG. 8: (a) $g_{bb}(r)$, (b) $g_{ss}(r)$ and (c) $g_{bs}(r)$ vs. r for N=144 and (d) $g_{bb}(r)$, (e) $g_{ss}(r)$ and (f) $g_{bs}(r)$ vs. r for N=4096.

The $\langle O_d \rangle$ vs βV_0 data for other system sizes are plotted in Fig. 9(a)-(b). I observe discontinuity in $\langle O_d \rangle$

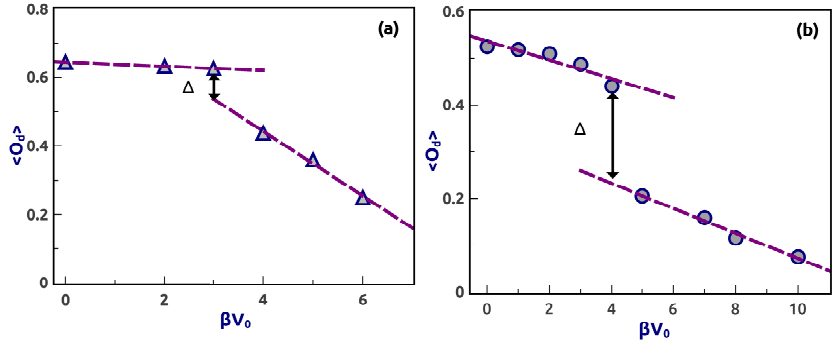

FIG. 9: Average order parameter $< O_d >$ vs. βV_0 for (a) N=144 and (b) N=4096.

for both the system sizes. The discontinuity (Δ) in order parameter depends on N as shown in Fig. 10(a). I observe that Δ increases (linearly) with N confirming a first order phase transition.

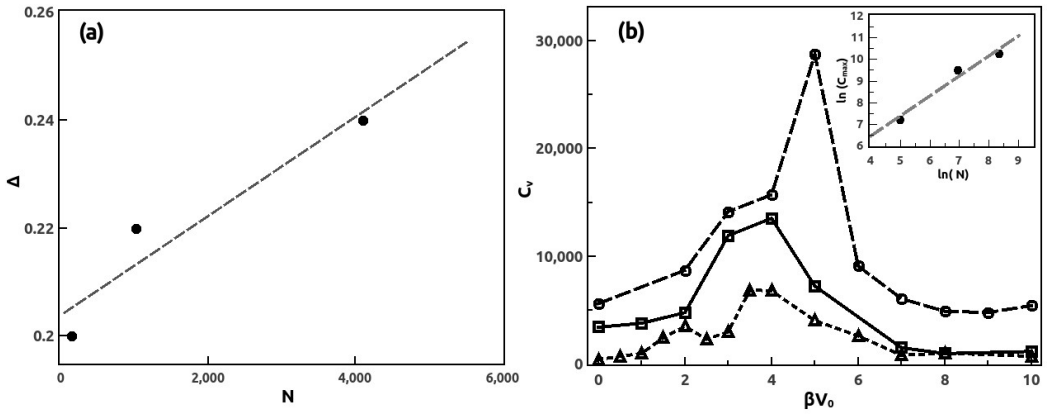

FIG. 10: (a) Discontinuity Δ vs. N. (b) Specific heat C_v vs. βV_0 for N=144(triangle, dotted line), N=1024(square, solid line), N=4096(circle, dashed line) with log-log fitting of heat capacity ln(C_{max}) vs. ln(N) in the inset with exponent 0.95.

I also examine the behaviour of the specific heat of the system, using the fluctuation of energy:

$$C_V = \frac{< (E - \bar{E}) >^2}{K_B T^2}, \tag{7}$$

Here E is the total energy at a given configuration and $\bar{E}$ is the average energy. Fig. 10(b) shows the C_V vs. βV_0 plot for N=1024. I observe peak in specific heat, C_{max} at βV_0=4.0 close to point of discontinuity P in $\langle O_d \rangle$. The peaks in specific heat shows slight shift similar to that in the point of discontinuity in the order parameter for different N. C_{max} is plotted against N in the inset of Fig. 10(b). The figure shows linear dependence on N, as in case of first order transition [18]. The, increase in Δ and C_{max} with N confirm that, system undergoes first order phase transition while going from a complete phase separated state to a mixed phase in presence of an external modulation potential.

Dynamic behaviour

I perform BD simulation strating from equilibriated MC configuration. I show snapshots from BD simulation at $\beta V_0 = 0.0$ and 10.0 in supplementary figure Fig. 10. I observe that the formation and breaking of clusters of

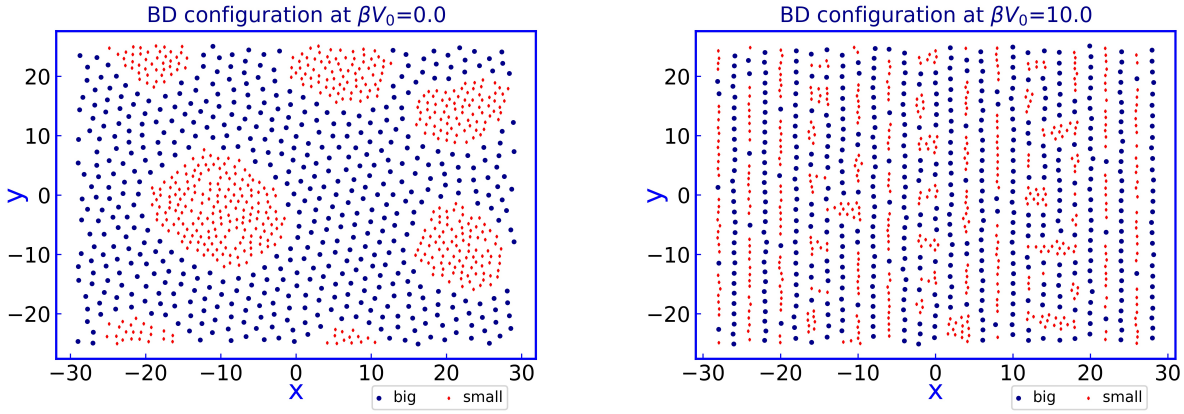

FIG. 11: Equilibrium BD configuratin for N=1024 at (a) $\beta V_0 = 0.0$, (b) $\beta V_0 = 10.0$.

smaller particles remain intact similar to MC simulation. The comparison between the BD and MC data are shown in Fig. 11(a)-(c) with respect to $g_{\alpha\beta}(r)$ at $\beta V_0 = 0.0$. I get similar results for both the simulations.

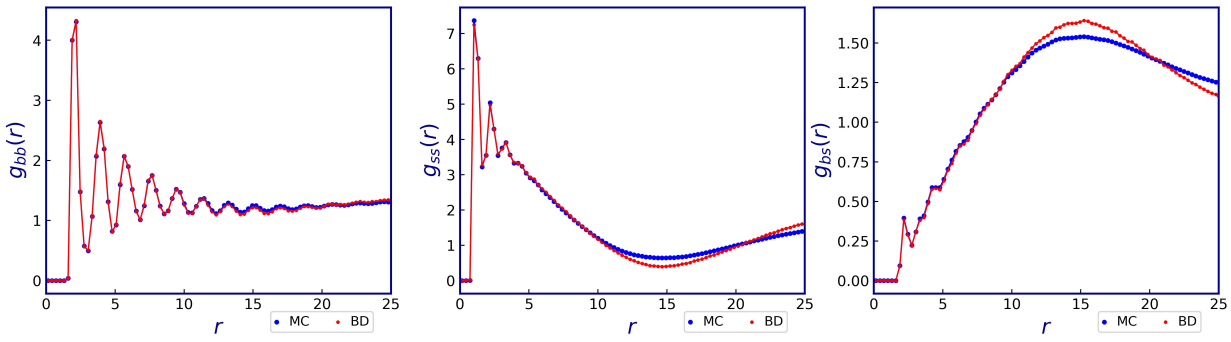

FIG. 12: BD and MC matching of rdf at $\beta V_0 = 0.0$ (a) $g_{bb}(r)$, (b) $g_{ss}(r)$ and (c) $g_{bs}(r)$ vs. r for N=1024.

Next I explore the dynamic behaviour using the BD trajectories accompanying the structural changes. MSD's along parallel and perpendicular direction $\langle(\Delta x_\alpha)^2\rangle$ and $\langle(\Delta y_\alpha)^2\rangle$ for both bigger and smaller particles (α =b, s) are plotted against time for different βV_0 in Figure 12.

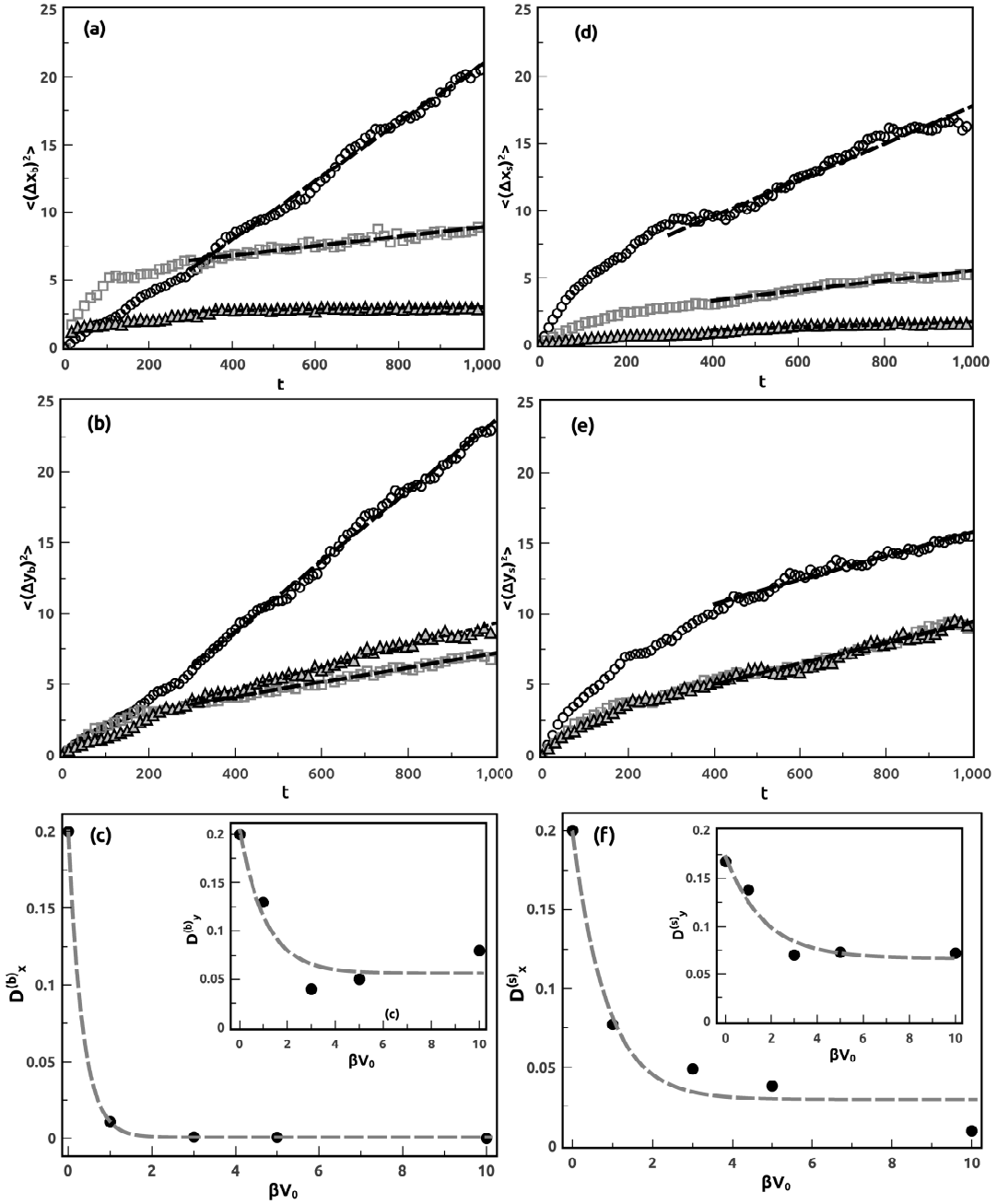

FIG. 13: (a) Mean square displacement of bigger particles along x-direction $\langle(\Delta x_b)^2\rangle$ for $\beta V_0 = 0.0$ (open circle), $\beta V_0 = 5.0$ (open square, data multiplied by 50), $\beta V_0 = 10.0$ (open triangle, data multiplied by 50). (b) Mean square displacement of bigger particles along y-direction $\langle(\Delta y_b)^2\rangle$ for $\beta V_0 = 0.0$ (open circle), $\beta V_0 = 5.0$ (open square), $\beta V_0 = 10.0$ (open triangle) (c) Diffudion coefficient $D_x^{(b)}$ from the long time slope of temporal dependence of MSD for bigger particles along x and $D_y^{(b)}$ vs. βV_0 (inset). (d) Mean square displacement of smaller particles along x-direction $\langle(\Delta x_s)^2\rangle$ for $\beta V_0 = 0.0$ (open circle), $\beta V_0 = 5.0$ (open square), $\beta V_0 = 10.0$ (open triangle). (e) Mean square displacement of smaller particles along y-direction $\langle(\Delta y_s)^2\rangle$ for $\beta V_0 = 0.0$ (open circle), $\beta V_0 = 5.0$ (open square), $\beta V_0 = 10.0$ (open triangle). (f) Diffusion coefficient $D_x^{(s)}$ from the long time slope of temporal dependence of MSD for bigger particles along x and $D_y^{(s)}$ vs. βV_0 (inset).

The MSD data for the big particles are shown in Figs. 12(a) and (b). I observe that in the demixed state ($\beta V_0 = 0.0$), $\langle(\Delta x_b)^2\rangle$ for the bigger particles increases linearly with time, characteristic of diffusive behaviour (Fig. 12(a)). $\langle(\Delta x_b)^2\rangle$ (Fig. 12(a)) shows weak dependence on time for $\beta V_0 = 5.0$, in the large time limit, reflecting strong pinning of the bigger particles at the potential minima. This is further enhanced as I increase $\beta V_0 (= 10.0)$ (Fig. 12(a)). Along the direction perpendicular to the modulation, $\langle(\Delta y_b)^2\rangle$ for the bigger particles show diffusive dynamics at $\beta V_0 = 0.0$ (Fig. 12(b)) similar to $\langle(\Delta x_b)^2\rangle$ in absence of external modulation. At $\beta V_0 = 5.0$ (Fig. 12(b)) and $\beta V_0 = 10.0$ (Fig. 12(b)) $\langle(\Delta y_\alpha)^2\rangle$ show decrease in slope. I compute the diffusion coefficients $D_x^{(b)}$ and $D_y^{(b)}$ from the long time slopes of $\langle(\Delta x_b)^2\rangle$ and $\langle(\Delta y_b)^2\rangle$ as shown in Fig. 12(a)-(b). I plot $D_x^{(b)}$ and $D_y^{(b)}$ vs. βV_0 in the main panel and inset of Fig. 12(c) respectively. I observe that initially at $\beta V_0 = 0.0$ the values are quite close to one another. But as the modulation increases in strength the diffusion becomes slow following exponential decay, $D_x^{(b)} = 0.18e^{-1.07\beta V_0}$. The inset shows that $D_y^{(b)}$, as a function of βV_0, behaves as $D_y^{(b)} = 0.18e^{-1.07(\beta V_0)}$.

$\langle(\Delta x_s)^2\rangle$ data are plotted against time in Fig. 12(d) for smaller particles. I observe diffusive behaviour in MSD in the long time limit. $\langle(\Delta y_s)^2\rangle$ in Fig. 12(e) for the smaller particles also show diffusive behaviour in longer time for all βV_0. This suggests that the smaller particles can move among the clusters particularly for low βV_0. I compute the diffusion coefficients $D_x^{(s)}$ and $D_y^{(s)}$ from the long time slopes of $\langle(\Delta x_s)^2\rangle$ and $\langle(\Delta y_s)^2\rangle$ for smaller particles. I plot $D_x^{(s)}$ and $D_y^{(s)}$ vs. βV_0 in the main panel and inset of Fig. 12(f) respectively. The smaller particles, like the bigger ones, also diffuse slowly as the strength of modulation increases and they are compelled to align themselves along the potential minima. The results are similar to my result of mono-dispersive colloidal particles described in chapter III. The smaller particles should have higher diffusion coefficients due to their smaller size. But here I observe their diffusion coefficient as slow as that of bigger ones. In low βV_0, the slow diffusion is due to their restrcited motion in the clusters. On the other hand when strength of modulation is high, the diffusion for the smaller particles decrease due to restricted motion along y-direction.

IV. CONCLUSION

To summarize, I show from MC simulations using various system sizes that a demixed binary colloid with particles of different sizes undergo mixing in presence of an external periodic modulation where the modulation wave

length matches with the bigger particles and higher strength of modulation. The changes in the mixing behaviour accompanies a first order phase transition. I further carry out BD simulations and show that the diffusion coefficients fall of for both species with modulation strength. Typically demixing is known to show phase coexistence ending in a critical point[19]. The critical point for demixing of binary colloids tuning the size ratio has been reported [20]. Shifting of critical point in case of a critical colloidal-liquid to colloidal-liquid demixing phase transition can be controlled by solvent temperature[21]. Demixing between phases in colloids with charge asymmetry is observed[2]. First order phase transition in demixing due to size asymmetry in colloids has been reported as well[22]. Unlike the earlier observations, I show that the miscibility of a binary colloid may be tuned by an external modulation. my studies show the possibility of tuning mixing property in a colloidal mixture by external modulation potential which maybe useful in areas where controlled mixing of the components is desirable as in drug industries, separation technology and so forth.

[1] P. D. Kaplan, A. G. Yodh, and D. J. Pine, Phys. Rev. Lett. **68**, 393 (1992).

[2] K. Yoshizawa *et.al.*, Soft Matter **8**, 11732-11736 (2012).

[3] J. H. J. Thijssen and P. S. Clegg, Soft Matter **6**, 1182-1190 (2010).

[4] D. Truzzolillo, J. Chem. Phys. **156**, 034904 (2022).

[5] R. F. Capellmann, A. Khisameeva, F. Platten and S. U. Egelhaaf, J. Chem. Phys. **148**, 114903 (2018).

[6] D. A. Stariolo and G. Fabricius, J. Chem. Phys. **125**, 064505 (2006).

[7] T. Narumi, S. V. Franklin *et. al.*, Soft Matter **7**, 1472-1482 (2011).

[8] E. Lzaro-Lzaro, J. A. Perera-Burgos *et. al.*, Phys. Rev. E **99**, 042603 (2019).

[9] I. Buttinoni, Z. A. Zell *et. al.*, Soft Matter **11**, 8313-8321 (2015).

[10] M. Rex M and H. Löwen, Phys. Rev. E **75**, 051402 (2007).

[11] S. Dutta and J. Chakrabarti, Phys. Chem. Chem. Phys. **22**, 17731-17737 (2020).

[12] S. Dutta and J. Chakrabarti, Soft Matter **14**, 4477-4482 (2018).

[13] H. Xiao, *et al.*, Powder technology **312**, 360-368 (2017).

[14] Oleg A. Vasilyev, S. Dietrich and S. Kondrat, Soft Matter **14** 586-596 (2018).

[15] Jean-Pierre Hansen and Ian R. McDonald, *Theory of Simple Liquids* (Academic Press, London (3rd eds., 2006).

[16] K. Loudiyi, B. J. Ackerson, Physica A **184**, 1 (1992).

[17] J. Chakrabarti, H. R. Krishnamurthy, A. K. Sood and S. Sengupta, Phys. Rev. Lett. **75**, 2232 (1995).

[18] K. Binder, Rep. Prog. Phys. **50**, 783 (1987).

[19] K. Binder, In: D. Li, (eds) *Demixing. Encyclopedia of Microfluidics and Nanofluidics.* (Springer, New York, NY, 2015).

[20] H. Kobayashi, Phy. Rev. E **104**, 044603 (2021).

[21] O. Zvyagolskaya *et. al.*, Eur. Phys. Lett. **96**, 28005 (2011).

[22] P. C. Hemmer and T. H. Marthinsen, Mol. Phy. **100**, 667-671 (2002).

Chapter 5: Kinetics in a modulated binary colloid

I. INTRODUCTION

Kinetics is the study of pathways through which a condensed matter system goes from one phase point to another in time through transient processes, involving evolution of variables in the system with time. Confocal microscopy [1–5] allows to image and track colloidal particles with high resolution. This makes kinetic studies by real time tracking of colloidal trajectory feasible.

Experiments and simulation studies on kinetics of phase transformation in colloids have been reported extensively. Phase transition kinetics of a colloid-polymer mixture, too, has been studied experimentally[6] which provide insights into the pathways whereby the samples, after homogenization, separate into macroscopically coexisting colloidal gas, liquid, and crystal regions. The existence of distinct kinetic regimes and free-energy landscape of the system has been investigated. Charge stabilized polystyrene spheres were supercooled initiallly in a gaslike system[7]. Neucleation occurrs in single or two-step with amorphous clusters. The metastable gas-liquid coexistence is meausred from free energies and observed increase in rate of neucleation in transient state. Experiments show[8, 9] that as supersaturation is increased, the rate of crystal nucleation goes through a maximum. Another experiment[10] shows that presence of hydrophobic amorphous organic aerosols leads to crystallization of aqueous inorganic microdroplets at high relative humidity. This is shown to be correlated with ion-specific surface interactions mediated by destabilizing water.

Simulations, too, have been used extensively in the past decades to study kinetics of a colloidal system showing aggregation and neucleation. Simulations of crystal nucleation in colloidal suspension with varying size distributions were reported earlier [11]. This study shows that the probability of formation of critical nuclei going through a maximum is achieved as the supersaturation is increased. This is observed due to an increase in supersaturation of the solidliquid interfacial free energy. Extensive Brownian dynamics simulations on the self-assembly of colloidal particles for a short-range attractive model that is quenched below its meta stable critical point has been reported[12]. It is reported that in the small volume fractionand low-temperature region the sticky beads diffuse around the system,

without reaching a final large cluster. For larger volume fractions in this low-temperature regime, a gel forms as the result of kinetically slowed down spinodal decomposition. A study characterises a two-dimensional amorphous binary colloidal assemblies composed of particles of two different sizes by the loss of hexagonal close-packing for larger particles, occurring when the size ratio between small and large particles exceeds a certain threshold value[13]. The computation has beed varied to probe various arrangements of particles. For moderately low particle number ratios large particles retain a denser arrangement with transitions from hexagonal symmetry to the coexistence of different types of symmetries. The aggregation of binary colloids of the same size and balanced charges is studied by Brownian dynamics simulations for dilute suspensions[14] that show that the formation of colloidal crystals is dominated by kinetic effects leading to the growth of well-ordered crystallites of the sodium-chloride (NaCl) and cesium-chloride (CsCl) bulk phase.

In chapter 4 I report a demixed binary mixture with different size ratio with mutual repulsive interaction leading to phase separation of the components in absence of external modulation. In presence of an external spatially periodic modulation, the system undergoes a first order phase transition to reach a modulated mixed state. Here I study the kinetics of the modulated colloidal binary mixture reported in Chapter 4 as the external modulation is turned off. I analyse the system in transient condition while going towards phase separated equilibrium state in absernce of the modulation. I analyse the cluster growth using cluster size distribution and morphology through the radius of gyration. I observe that the average sizes of the clusters grow in time as a power law with exponent 0.96 before saturating at the new equilibrium. The aspect ratio of the radius of gyration along the x and y-directions suggests that the clusters initially stretched along y-direction take circular shape as time progresses. I further look into mean square displacement and compute the diffusion coefficients for both the type of particles. I find diffusive dynamics for the type of particles in longer time. I observe faster diffusion in case of bigger particles, whereas the smaller particles show slow diffusion leading to aging of the clusters.

This chapter is organised as follows: I briefly describe the simulation protocol in section II. I discuss the time dependent structural properties like configuration, cluster size distribution, morphology and demixing order parameter

in section III followed by their dynamic properties in section IV. Section V concludes the chapter.

II. SIMULATION PROTOCOL

The model system is similar to that described in Chapter 4. I fix $\frac{\epsilon_{bb}}{K_BT} = \frac{\epsilon_{ss}}{K_BT} = 1.0$ and $\frac{\epsilon_{bs}}{K_BT} = 1.5$. I take upon the modulated mixed phase at $\beta V_0 = 10.0$ as illustrated in Fig. 1(d) in Chapter 4 and switch off the external modulation starting from this equilibrium and run BD simulation until new equilibrium is reached. I run for a total of 10^7 BD steps taking integration time step $\Delta t = 0.001\tau_B$. Since the system is contineously evolving in transient state, averaging of different quantities over time is not possible. So, all the time dependent quantities of interests are calculated over forty independent BD trajectories with different initial modulated structures at a given time.

III. TIME DEPENDENT STRUCTURAL CHANGES

I start from modulated equilibrium configuration at high modulation ($\beta V_0 = 10.0$), obtained from my previous report, as shown in Fig. 1(d) of Chapter 4. Then I switch off the external modulation and evolve the system in time

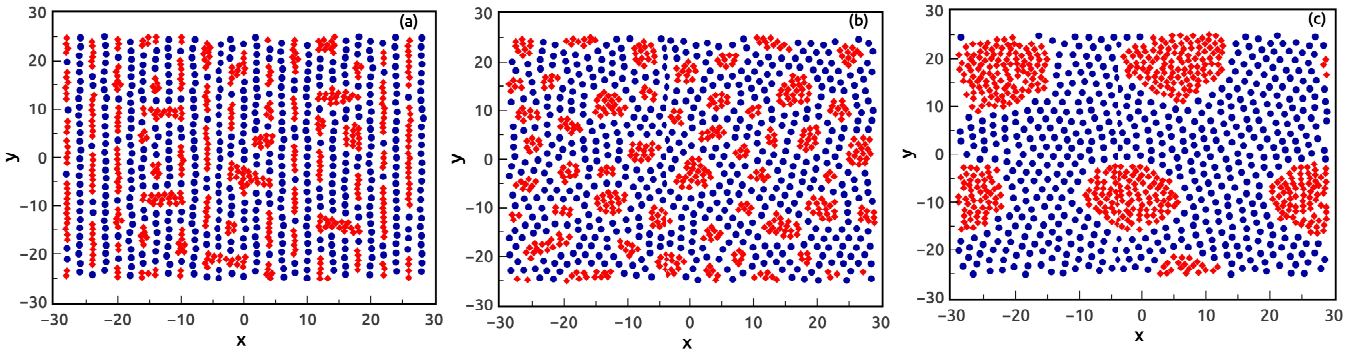

FIG. 1: Final configuration strating from $\beta V_0 = 10.0$, at (a) initial time $t_0 = 0.0$ (b) intermediate time $t_0 = 30.0$ and (c) time when system has reached equilibrium $t_0 = 100.0$.

using BD simulation. Now, let us consider the time evolution of the system. I observe that as time progresses, due to absence of modulation, bigger particles now have freedom to move in the whole phase spcae and more smaller

particles are coming together to form clusters as shown in Fig. 1(b). The final configuration after the system has reached equilibrium is shown in Fig 1(c). I observe big clusters of smaller particles are formed in a background of the bigger particles. Hence, the system has reached a phase separated state. This is similar to my observation in chapter 4.

Next I describe the system in transient condition from the initial mixed modulated phase to phase separated phase in absence of modulation. I characterize structural changes by computing average cluster sizes of the smaller particles with time. I consider two small particles to belong to a cluster whose centre to centre distances in x- and y-direction are less than x_{cl} and y_{cl} respectively. I choose $x_{cl} = 1.25$, $y_{cl} = \frac{\sqrt{3}}{2}x_{cl}$ as explained in Chapter 4. I plot the mean cluster size $\langle C(t)\rangle$ versus t in Fig. 2(a). I observe that the cluster size increases linearly in t before saturating

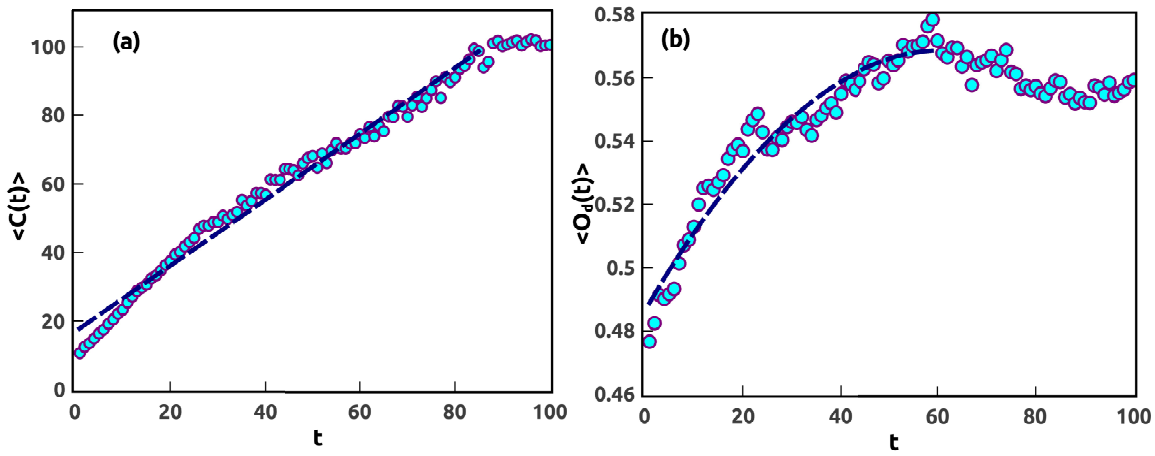

FIG. 2: Average cluster size $\langle C(t)\rangle$ vs. t plot. The dashed line shows the linear fitting with dependence $\langle C(t)\rangle \sim t^{0.96}$. (b) Order parameter $\langle O_d(t)\rangle$ vs. t plot with fitting of the growth shown in blue dashed line with dependence $\langle O_d(t)\rangle \sim t^{0.2}$.

to a large value as the system reaches equilibrium for $\beta V_0 = 0.0$ shown by the dashed line. I define the transient time by the time where the mean cluster size is half of that in equilibrium value. Here the transient time is observed as $T_s = 40$.

I calculate the time dependent demixing order parameter $\langle O_d(t)\rangle$ for different βV_0 as explained in Chapter 4:

Fig. 2(b) shows the order parameter averaged over independent runs $\langle O_d(t)\rangle$ vs t. I observe that $\langle O_d(t)\rangle$ increases with t gradually as time progresses and finally saturates as the system reaches new equilibrium. This happens because

now the particles are trying to reside in the vicinity of their similar kind, thus gradually yielding higher $\langle O_d(t)\rangle$ values. The order parameter follows a power law dependence as $\langle O_d(t)\rangle = 0.46t^{0.2}$.

I also examine the shape of the clusters. I calculate the radius of gyration for both x and y-direction from the centre of mass frame:

$$\langle x_G(t)\rangle = \langle\sqrt{\frac{\Sigma(x_i(t) - x_{CM}(t))^2}{N}}\rangle \tag{1}$$

$$\langle y_G(t)\rangle = \langle\sqrt{\frac{\Sigma(y_i(t) - y_{CM}(t))^2}{N}}\rangle, \tag{2}$$

where $x_{CM}(t)$ and $y_{CM}(t)$ are the centre of masses of the clusters along x and y-direction respectively at a given time t. I plot the aspect ratio $\langle A_G\rangle = \frac{\langle x_G(t)\rangle}{\langle y_G(t)\rangle}$ in Fig. 3. I observe that, $A_s = 1.33t^{0.15}$ grows until $t = 30.0$. The smaller particles from elongated clusters along y-direction initially. Then the clusters form slight bulging in the x-direction at time progresses and finally it approaches unity corresponding to circular clusters as the system reaches equilibrium.

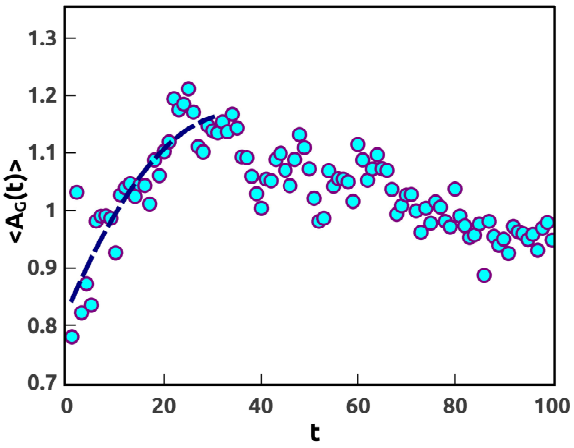

FIG. 3: $\langle A_G(t)\rangle$ vs. t plot with fitting shown in dashed line with exponent 0.15.

IV. DYNAMICAL BEHAVIOUR

I also look into the dynamical behaviour of the particles in the transition state. I calculate MSD for both bigger and smaller particles starting from different initial time t_0 during the transition state. Since the system is evolving in

time, one can not average over t_0 and thus t_0 remains a parameter. The MSDs of the big prticles for a given choice of t_0 are defined as:

$$\langle(\Delta r; t_0)_b^2\rangle = \langle\frac{1}{N}\Sigma_i[(x_{ib}(t) - x_{ib}(t_0))^2 + (y_{ib}(t) - y_{ib}(t_0))^2]\rangle. \tag{3}$$

and similarly for the small particles:

$$\langle(\Delta r; t_0)_s^2\rangle = \langle\frac{1}{N}\Sigma_i[(x_{is}(t) - x_{is}(t_0))^2 + (y_{is}(t) - y_{is}(t_0))^2]\rangle. \tag{4}$$

I show MSD for the bigger particles $\langle(\Delta r; t_0)_b^2\rangle$ for different t_0 in Fig. 4(a). I observe that the dynamics for the bigger particles is diffusive. I calculate the diffusion coefficient for the bigger particles $D_b(t_0)$ from the slope of the MSDs and plot them against t in Fig. 4(b) for different t_0. I observe that $D_b(t_0)$ increases linearly with t_0. In absence of external modulation, the bigger particles have more freedom and hence, undergo faster diffusion.

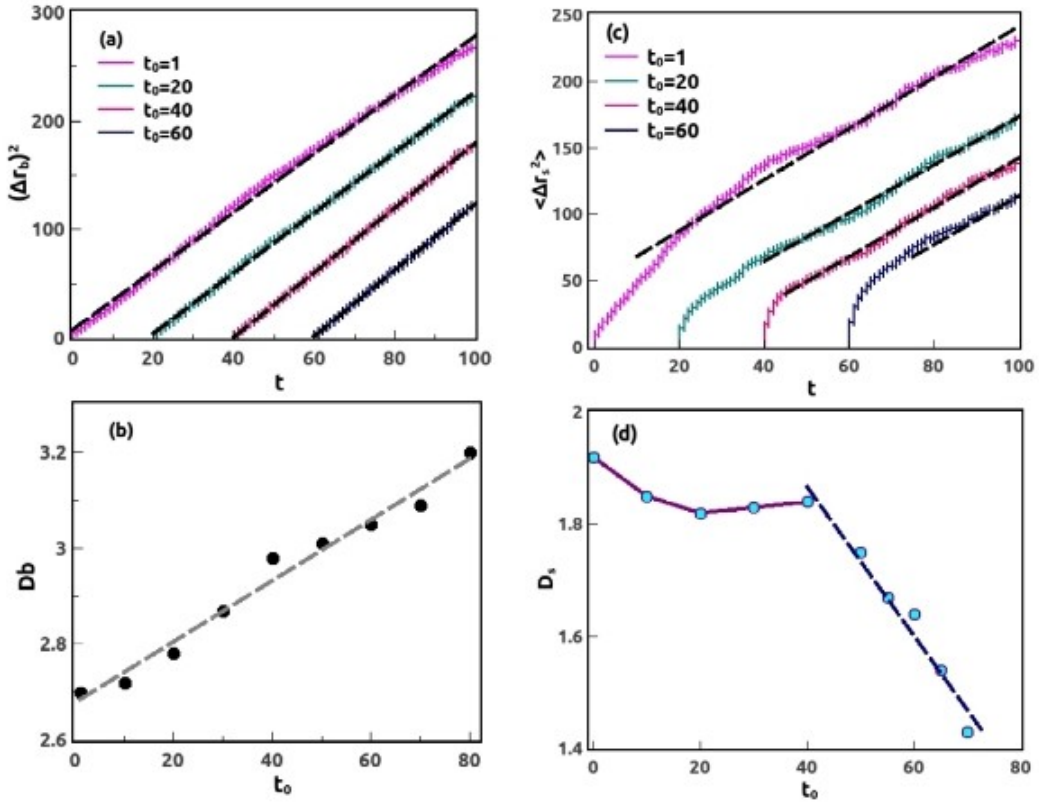

FIG. 4: (a) $\langle(\Delta r)_b^2\rangle$ vs. t_0 plot. For various t_0, the dashed lines are the best linear fits. (b) D_b vs. t_0 plot. Dashed line shows linear fit (c) $\langle(\Delta r)_s^2\rangle$ vs. t plot. For various t_0, the dashed lines are the best linear fits in the large time limit. (d) D_s vs. t plot. The solid line is a guide to the eyes. The dashed line is the best lineasr fit for larger t_0 with dependence $D_s = 2.4 - 0.01t_0$.

Next I plot MSD for the smaller particles $\langle(\Delta r; t_0)_s^2\rangle$ for different t_0 in Fig. 4(c). I obtain for the long time linear fitting of this MSD data as shown in Fig. 4(c). I calculate the diffusion coefficient for the smaller particles D_s from long time slope of the MSDs starting from different times and plot them against t_0 in Fig. 4(d). I observe that initially $D_s(t_0)$ does not depend significantly on t upto $t_0 \simeq T_s$ and then falls linearly with time. So, initially the dynamics is slow but steady due to formation of clusters ongoing in the system. Then difussion of the smaller particles becomes very slow because of their restricted motion within the clusters.

V. CONCLUSION

I study the system using BD simulations to explore the kinetics of transition time as a modulated binary misture reaches demixed state in equilibrium as the modulation is turned off. I observe formation of gradually large clusters of smaller particles in absence of external modulation. I also observe the aspect ratio to approach unity and saturation in demixing order parameter in transient time. I observe faster diffusion dynamics of bigger particles and slower diffusivity with observation time for smaller particles.

[1] V. Prasad, D. Semwogerere, and E. R. Weeks, Journal of Physics: Condensed Matter **19**, 113102 (2007).

[2] Dinsmore, D. Anthony, *et al.*, Applied optics **40** 4152-4159 (2001).

[3] M. C. Jenkins, and S. U. Egelhaaf, Advances in colloid and interface science **136 2** 65-92 (2008).

[4] M. H. Chestnut, Current opinion in colloid & interface science **2** 158-161 (1997).

[5] C. P. Royall, Ard A. Louis, and H. Tanaka, The Journal of chemical physics **127** (2007).

[6] V. J. Anderson, and H. NW Lekkerkerker, Nature **416** 811-815 (2002).

[7] J. R. Savage and A. D. Dinsmore *Phys. Rev. Lett.* **102**, 198302 (2009)

[8] K. F. Kelton, *Solid State Physics* **45** (eds Ehrenreich, H. & Turnbull, D.) 75178 (Academic, New York, 1991).

[9] P. Pusey, *Liquids, Freezing and Glass Transition* (eds Hansen, J. P., Levesque, D. & Zinn-Justin, J.) 763931 (North-Holland, Amsterdam, 1991).

[10] D. Davis Ryan and A. T. Margaret *Science Advances* **3**, (2017).

[11] S. Auer, D. Frenkel, Nature **413**, 711713

[12] Sumedh R. Risbud, and W. Swan. James, Soft Matter **11** 3232-3240 (2015).

[13] V. Lotito, and Z. Tomaso, Nanomaterials **9** 921 (2019).

[14] T. Oncsik, *et al.*, Langmuir **30** 733-741 (2014).

[15] A. Brengere, D. Bonn, and J. Meunier, Physical Review E **64** 021510 (2001).

[16] J. M. Lynch, C. C. Gianguido and E. R. Weeks, Physical Review E **78** 031410 (2008).

[17] L. Cipelletti, *et al.*, Physical review letters **84** 2275 (2008).

[18] Wang, Yang, *et al.* Environmental science & technology **53** 8136-8146 (2019).

[19] Li, Qi, X. Peng, and Gregory B. McKenna, Soft Matter **13** 1396-1404 (2017).

[20] Siddique J. Khan, C. M. Sorensen, and A. Chakrabarti, The Journal of chemical physics **131** (2009).

[21] Cao, Tianchi, *et al.*, Physical Chemistry Chemical Physics **19** 15160-15171 (2017).

[22] Evans, R. M. L., W. C. K. Poon, and F. Renth, Physical Review E **64** : 031403 (2001).

Chapter 6: Summary and outlook

This thesis reports studies on colloidal systems under modulation. Despite wide range of past studies, dynamics of particle under modulation have not been well explored earlier. I explore dynamics of colloids under different contexts.

Firstly, I study the dynamics of a modulated mono-dispersieve colloidal system. As the system is subjected to an external spatially periodic modulation in one direction, the anisotropy caused by this modulation makes the motion along that direction sub-diffusive. The crowding particles along the potential minima hinder the motion in transverse direction. The dynamical heterogeneity in modulated colloids has not been reported so far to the best of my knowledge. Such dynamic heterogeneity may be explored in experiments by measuring the self-van Hove function through neutron scattering and direct video microscopy. It will be interesting to study mechanical and flow properties of modulated systems. Such studies may prove useful to design systems with targetted mechanical properties.

Next I take up a system of binary mixture having different size ratio and mutual interaction strength in an external modulation. I apply a one-dimensional spatially periodic external modulation with two different strength for two different species in a binary colloidal system. In the absence of the external potential the binary system phase separates, having big clusters of smaller particles in a background of bigger ones due to internal cross-species repulsion. In presence of the external modulation, the bigger particles align themselves along the potential minima due to matching of their diameter with the external potential by making their way through the clusters of the smaller particles and resulting in mixed modulated state of big and small particles. state. The thermodynamic quantities, like the de-mixing order parameter and the specific heat show that the mixing is accompanied by a first order phase transition with a jump in de-mixing order parameter.

I further explore the kinetics of cluster growth as I switch off the external modulation. I start from a mixed state as otained earlier for a high strength of modulation and let the system elvolve in time using BD simulation. I characterise different quantities in transient state. I observe increase in cluster size, radii of gyration and demixing order parameter before coming to saturation as the system reaches equilibrium. I observe faster dynamics for the bigger particles and

slower for smaller particles within the clusters. Few of many interesting future work based on this study can be to look into phase diagram and dynamics experimentally. Despite elaborate studies on binary mixing-de-mixing phenomena, there has been no study on phase transition or its order, associated with this mixing induced by a spatially periodic external potential. my results suggest that mixing in a binary colloidal system can be tuned by external potential. The smaller particles form dynamically slower clusters in background of faster partiles in the demixed state in absence of external potential. These may be of importance in areas where controlled mixing of the components is desirable as in drug industries, separation technology, fabrication of novel materials with tailored mechanical properties.